EES Batteries

REVIEW

View Article Online
View Journal | View Issue

Cite this: *EES Batteries*, 2026, **2**, 377

Toward next-generation cathodes for lithium-ion batteries: progress and prospects of single-crystal lithium-rich manganese-based oxides

Teng Yang,†[a,b] Jinyang Dong,†[a,c] Yuefeng Su,*[a,b,c] Huiquan Che,[a] Yun Lu,[a,c] Jianan Hao,[a,c] Ning Li,[a,b,c] Yibiao Guan,*[d] Lai Chen*[a,c] and Feng Wu[a,c]

Amid global efforts to achieve green economy and accelerate sustainable energy transformation, lithium-ion batteries have become a cornerstone for electric transportation and stationary storage systems. To meet increasing requirements for energy density, cycling durability, and operational safety, the development of high-performance cathode materials is critical. Single-crystal lithium-rich manganese-based layered oxides (SCLRMs) have gained increasing attention owing to their high specific capacity, structural coherence, and favorable interfacial stability. This review summarizes recent progress in the controlled synthesis, structural regulation, and performance optimization of SCLRMs. Key modification strategies, including compositional modification, surface engineering, and morphology design, are evaluated with respect to their roles in enhancing electrochemical behavior and suppressing degradation. Emphasis is placed on the integration of multi-dimensional and multi-scale characterization techniques to elucidate the evolution of nanoscale architectures, interfacial chemistry, and redox mechanisms during operation. Furthermore, artificial intelligence (AI) assisted approaches are highlighted for their potential in accelerating materials discovery and guiding performance-driven design. These developments are expected to enable the integration of SCLRMs into next-generation battery frameworks that not only exhibit high energy density and long cycle life but also support the emergence of smart battery systems with enhanced reliability, safety, and autonomous diagnostic capabilities. By consolidating recent advancements and outlining core challenges, this review provides critical insights into the progress and prospects of SCLRMs as next-generation cathode materials for lithium-ion batteries.

Received 10th September 2025,
Accepted 11th December 2025

DOI: 10.1039/d5eb00167f

rsc.li/EESBatteries

Broader context

Lithium-ion batteries (LIBs) have become the dominant technology for energy storage in fields ranging from portable electronics to electric vehicles and grid applications. Their continued advancement relies heavily on the development of cathode materials, which determine performance and cost. Lithium-rich manganese-based oxides (LRMs) are considered among the most promising candidates because of their high specific capacity and the abundance of manganese, making them attractive for large-scale deployment. Nevertheless, conventional polycrystalline LRMs suffer from low initial efficiency, voltage decay, capacity fading, and limited rate capability, which restrict their practical application. Recent studies have demonstrated that single-crystal LRMs (SCLRMs), with their coherent structure and absence of grain boundaries, can mitigate many of these problems by improving structural integrity, ion transport, and interfacial stability. Various modification strategies, including elemental doping, surface coatings, and morphology control, have been explored to further enhance their mechanical and electrochemical performance. Looking to the future, the integration of SCLRMs into solid-state batteries may significantly improve safety and energy density, while intelligent battery systems represent an emerging direction for adaptive energy storage. At the same time, careful investigation of degradation mechanisms remains essential to guide rational design. This review highlights recent progress and challenges in SCLRM research, aiming to provide insights that support the development of next-generation LIBs and contribute to sustainable energy strategies worldwide.

[a]*School of Materials Science and Engineering, Beijing Key Laboratory of Environmental Science and Engineering, Beijing Institute of Technology, Beijing 100081, P.R. China. E-mail: suyuefeng@bit.edu.cn, chenlai144@sina.com*
[b]*Beijing Institute of Technology Zhuhai Campus, Zhuhai 519085, P.R. China*
[c]*Chongqing Innovation Center, Beijing Institute of Technology, Chongqing, 401120, P.R. China*
[d]*National Key Laboratory of Renewable Energy Grid-Integration, China Electric Power Research Institute, Beijing 100192, P.R. China. E-mail: guanyb@epri.sgcc.com.cn*
† These authors contributed equally to this work.

1. Introduction

Lithium-ion batteries have become the dominant energy storage technology due to their high energy density, long cycle life, and superior charge–discharge efficiency, making them indispensable for applications in portable electronics and large-scale energy systems. With the rapid growth of electric mobility and digital infrastructure, improving battery performance has emerged as a pressing scientific and industrial chal-

lenge.[1] Among the various components, the cathode material plays a decisive role in determining the electrochemical characteristics of the battery. Cobalt-based layered oxides are favored for their high tap density and elevated operating voltage.[2,3] However, their large-scale adoption is increasingly constrained by high cost, limited supply, and geopolitical concerns related to cobalt sourcing. Consequently, cobalt-lean and cobalt-free materials are gaining attention. Among these, $LiFePO_4$ has attracted significant interest due to its low cost, environmental compatibility, thermal stability, and long-term cycling reliability.[4] Nonetheless, its relatively low operating voltage and limited Li^+ diffusion, inherent to its olivine structure, restrict its energy density and high rate capability.[5] Moreover, its poor intrinsic electronic conductivity further limits performance under demanding operating conditions. On the other hand, high-nickel layered cathodes such as NCM811 and NCA offer higher specific capacities and energy density owing to the increased redox activity of nickel, but they suffer from surface instability, thermal decomposition, and rapid degradation during prolonged cycling or high-voltage operation.[6,7] These contrasting characteristics illustrate the trade-offs between structural stability, energy output, and material cost across different cathode systems. While anode materials such as graphite and silicon have demonstrated substantial improvements in theoretical capacity, the cathode remains the limiting factor in enhancing the overall energy density of Li^+ batteries.[8,9] This technological urgency is echoed in strategic battery development programs launched globally. National roadmaps including China's battery strategy, the United States' Battery500 initiative, the European Union's BATTERY 2030+, and Japan's RISING II project have all proposed ambitious targets for next-generation battery systems, such as reaching specific energy densities of 500 Wh kg^{-1} within defined industrial timelines.[10–13] These policy frameworks reflect a growing consensus that improvements in cathode chemistry are essential for supporting the large-scale deployment of electric vehicles and sustainable energy infrastructure. The discrepancy underscores the critical importance of developing cathode materials that integrate high specific capacity, stable electrochemical performance, cost-effective synthesis, and compatibility with large-scale production. Therefore, the rational design and scalable fabrication of low-cost, high-energy-density cathode materials represent a key direction in the advancement of next-generation Li^+ battery technologies.

Lithium-rich manganese-based layered oxides (LRMs) have garnered widespread attention as advanced cathode materials owing to their exceptional specific capacity exceeding 250 mAh g^{-1} and ability to deliver strong discharge currents, as illustrated in Fig. 1a. Their large-scale applicability is further supported by the high natural abundance and low cost of manganese, making them economically viable for industrial deployment.[14] As shown in Fig. 1b, research activity in this field has significantly expanded over the past decade, driven by the need for cathodes that combine high energy density with sustainable material supply. Among LRMs, lithium-rich nickel–manganese–cobalt oxides (Li-rich NMCs) are particularly notable for achieving capacities approaching 300 mAh g^{-1} and a theoretical material-level energy density close to 1000 Wh kg^{-1} *versus* Li/Li^+.[15] These materials retain the layered framework of conventional NMCs but incorporate excess lithium in the transition metal (TM) layer, where Li^+ replaces TM cations in an ordered honeycomb arrangement. Despite their relatively low tap density and limited volumetric energy density, LRMs demonstrate a favorable balance among gravimetric energy density, cycling durability, and cost-effectiveness, making them highly promising for automotive and grid applications (Fig. 1c).[16] However, their practical volumetric energy density remains lower than that of Ni-rich layered oxides, though still outperforming their $LiFePO_4$ and $LiMn_2O_4$ counterparts (Fig. 1d).[17] This limitation is primarily due to their low material density, which results from the excessive incorporation of lithium, an element with low atomic weight, replacing heavier TM at octahedral sites. In addition, the low tap density of Li-rich NMCs also partially stems from the porosities of the particles generated upon the decomposition of carbonate precursors.[18] Beyond these structural factors, several intrinsic limitations hinder their practical application in advanced Li^+ batteries. First, LRMs suffer from significant capacity and voltage decay during long-term use, resulting in the energy density rapidly decreasing with cycling.[19,20] Second, they exhibit relatively poor initial coulombic efficiency and suffer from irreversible capacity loss in the first cycle due to structural rearrangement and parasitic reactions.[21] Third, LRMs have poor rate performance, which affects their ability to meet high-power application requirements. Fourth, at elevated temperatures, they are prone to oxygen release and gas evolution, causing electrode expansion and interfacial instability.[22] Fifth, under extreme conditions such as overcharging and over-discharging, they can experience thermal runaway and structural degradation.[23–25] While these challenges remain, the substantial advantages of LRMs in terms of capacity, elemental abundance, and cost still support their continued exploration (Fig. 1e). Further optimization of structural design and synthesis strategies, and understanding of the degradation mechanism will be essential for improving their performance and accelerating their translation into practical battery systems.

In light of the unresolved challenges associated with traditional polycrystalline lithium-rich manganese-based layered oxides (PCLRMs), including structural instability, interfacial degradation, and thermal sensitivity, growing research efforts since the early 2010s have turned toward the development of SCLRMs as a potentially advantageous alternative.[26–28] Single-crystal (SC) cathode materials, characterized by their continuous, grain-boundary-free architecture, are anticipated to alleviate many of the mechanical and electrochemical issues observed in their polycrystalline (PC) counterparts.[29] The absence of grain boundaries is expected to suppress intergranular cracking and particle fracture during repeated cycling, thereby enhancing structural integrity and contributing to improved capacity retention and reduced voltage decay.[30]

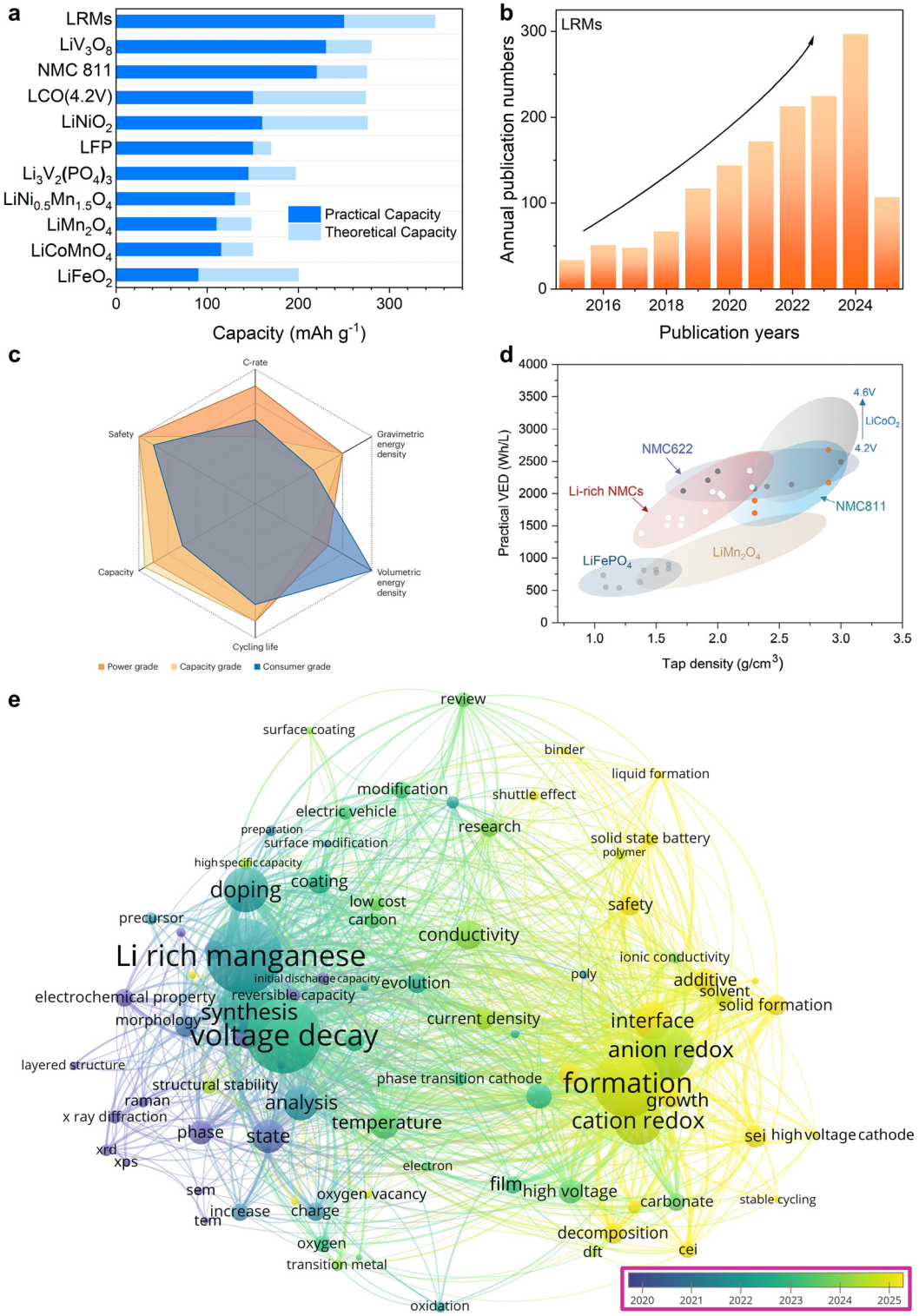

Fig. 1 Concentrate on LRMs. (a) Capacity comparison of prototypical cathode materials. (b) Trend of annual publication numbers for LRMs from 2015 to 2025. (c) Main considerations of Li^+ batteries in power-grade, capacity-grade, and consumer-grade battery segments. Reproduced from ref. 16, copyright 2025 NPG. (d) Volumetric energy density *versus* tap density for the classical cathode material. Reproduced from ref. 17, copyright 2024 Wiley-VCH. (e) Research hotspots of LRMs. Data are from Web of Science.

Additionally, SC structures are thought to promote more uniform Li^+ diffusion and uninterrupted electronic conduction, which may enhance rate capability and reduce polarization under high-rate operation.[31] Homogeneous ion transport is also believed to mitigate local overpotentials and electrolyte degradation, leading to lower gas evolution and improved interfacial stability at elevated temperatures.[32,33] From a thermal safety perspective, the compact and coherent structure of SC particles is considered more resistant to oxygen evolution and thermal runaway.[34] Beyond these electrochemical advantages, the development of SC architectures may also bring engineering benefits, particularly in tailoring particle morphology, size distribution, and surface texture to improve electrode processability.[35] Such structural control is expected to contribute to enhanced tap density and better electrode-level packing performance, which are critical parameters for achieving high volumetric energy density. While further validation is required, current studies suggest that SCLRMs offer a promising direction for overcoming key limitations of PCLRMs and may serve as a structurally stable and scalable platform for the advancement of next-generation Li^+ battery cathodes.

While SCLRMs have demonstrated clear advantages in structural integrity, interfacial stability, and electrochemical reversibility, most existing studies in this field remain concentrated on PCLRMs, particularly in relation to redox mechanisms, phase evolution, and surface degradation. In contrast, systematic evaluation and integration of progress on SCLRMs have been relatively limited, despite their growing relevance in next-generation battery systems. This lack of a comprehensive review has hindered the formulation of coherent development strategies and the identification of unresolved technical barriers. To address this gap, the present review focuses specifically on the current status, key challenges, and future prospects of SCLRMs. This review is organized in the following manner. Section 2 outlines the development history and synthetic strategies of SCLRMs. Section 3 provides a comparative analysis of the physicochemical characteristics and electrochemical behaviors between SC and PC counterparts. Section 4 introduces representative modification strategies, including doping, surface coating, and structural design. Section 5 reviews the integration of SCLRMs into solid-state battery configurations. Section 6 focuses on diagnostic techniques developed for conventional lithium-rich systems and demonstrates their applicability to structural and interfacial characterization of SCLRMs. Section 7 presents the role of AI in battery research with a forward-looking perspective on its potential for SCLRM design, interface optimization, and smart system development. Finally, section 8 outlines our perspective on future development trends. Looking forward, we emphasize that a deeper mechanistic understanding of long-term degradation phenomena and dynamic interface evolution is essential for unlocking the practical potential of SCLRMs. Moreover, the adoption of AI-assisted analysis and high-throughput characterization is expected to accelerate material optimization and system-level integration. By consolidating existing progress and proposing forward-looking insights, this review aims to provide a timely and focused reference for guiding the rational design and application of SCLRMs in high-energy, high-stability Li^+ and solid-state battery technologies.

2. Development history and synthetic strategies

The development of LRMs has evolved through distinct phases since their conceptual origin in the early 1990s (Fig. 2). The pioneering work of Rossouw and Thackeray in 1991 first demonstrated that Li_2MnO_3 could be chemically activated to form layered lithium–manganese–oxide compounds with capacities approaching 200 mAh g^{-1}, highlighting the potential of Li–Mn–O systems for high-energy Li^+ batteries.[36] This initiated the structural foundation for LRMs, which was further advanced by Sakaki and Numata in 1997 and 1999 through the design of $LiCoO_2$–Li_2MnO_3 solid solutions. These compositions, described by $Li(Co_{1-x}Li_{x/3}Mn_{2x/3})O_2$, demonstrated homogeneous cation distribution and introduced the concept of excess lithium in the TM layer, forming the basis of what later became known as the solid solution model.[37,38] Interest in LRMs surged following a 2002 report by Dahn *et al.*, which showed that $Li[Ni_xLi_{(1-2x)/3}Mn_{(2-x)/3}]O_2$ materials delivered anomalously high capacities (>225 mAh g^{-1}), sparking intense research into their underlying charge compensation mechanisms.[39] In parallel, Thackeray *et al.* proposed a two-phase composite model expressed as $xLi_2MnO_3{\cdot}(1-x)LiTMO_2$, describing LRMs as nanocomposites of $LiMO_2$ and Li_2MnO_3 domains. These differing structural interpretations were often attributed to synthesis variables such as lithium content, calcination temperature, and time.[40] A breakthrough in mechanistic understanding came in 2006 when Bruce and Thackeray's team, through *in situ* differential electrochemical mass spectrometry (DEMS) and neutron diffraction, provided direct evidence for lattice oxygen loss and TM migration in Li $[Ni_{0.2}Li_{0.2}Mn_{0.6}]O_2$ during charging, validating the anionic redox hypothesis.[41] This shifted the design paradigm of LRMs from purely cationic redox to hybrid anion–cation redox frameworks. However, practical limitations such as oxygen evolution, voltage fade, and phase transformation during cycling prompted deeper exploration into microstructural and morphological strategies in the following decade.

In response to the structural and interfacial challenges facing conventional PCLRMs, SCLRMs have gained attention. Beginning in 2016, several studies began to explore the potential of SC design as a means to improve the structural and interfacial stability of LRMs. Wang and co-workers reported one of the earliest syntheses of submicron-scale SCLRMs, highlighting their morphological uniformity and crystallographic coherence.[26] In 2017, Kuppan and Chen's team systematically investigated the role of surface orientation using well-defined SCLRM particles, revealing that facet-dependent reactivity significantly influenced surface phase transformation and TM reduction, even prior to electrochemical cycling.[27] Li and colleagues in 2019 introduced a compo-

sitional gradient into SC particles using a molten salt treatment. This approach produced a depth-dependent lithium distribution that helped stabilize the lattice and mitigate oxygen-related degradation.[42] In 2021, Zhou and collaborators provided a direct comparison between PC and SC forms of Li-rich layered oxides, demonstrating that SC particles exhibited more stable structural evolution and fewer signs of microstructural damage during cycling.[43] Subsequently, in 2022, Sun and Zhang extended the application of SCLRMs to all-solid-state battery (ASSB) systems. Their findings suggested that the dense morphology and reduced surface oxygen activity of SC were beneficial for suppressing interfacial degradation at the solid electrolyte interface.[44] These representative works collectively illustrate a gradual progression in SCLRM research, transitioning from fundamental morphological design and surface chemistry investigation to performance validation under both liquid and solid-state electrochemical environments. Nevertheless, the SC route is not a perfect solution. Challenges such as synthesis scalability, control of particle size distribution, and incomplete stabilization of the oxygen redox process remain unresolved. Future studies should aim to integrate SC design with complementary structural and interfacial engineering approaches. The integration should be supported by in-depth mechanistic understanding and evaluation under practical full-cell conditions, in order to realize the full potential of lithium-rich cathode systems in advanced battery applications.

Since the early 2010s, SCLRMs have attracted growing attention due to their potential to mitigate bulk structural degradation and prolong the service life of high-energy Li^+ batteries. In initial studies, conventional synthetic routes such as co-precipitation, sol–gel processing, and molten-salt methods yielded submicron-sized particles, frequently smaller than 400 nanometers. These small particle sizes limited the mechanical and interfacial advantages typically associated with SC structures. In response, researchers have sought to refine these techniques to facilitate the formation of larger, well-faceted crystals with enhanced phase purity and size uniformity. Among traditional approaches, the co-precipitation method (Fig. 3a) remains widely utilized owing to its low cost, scalability, and capacity for homogeneous precursor formation.[45] In this technique, multiple metal ions are simultaneously precipitated from solution, followed by filtration, drying, and calcination to yield the final cathode material. However, when targeting SC formation, the process must be carefully controlled to prevent excessive nucleation and to promote anisotropic grain growth. Specific conditions such as low supersaturation, precise pH regulation, and extended thermal aging of the precipitate are essential for reducing defect density and improving crystallinity. But this method offers advantages in elemental doping. A long-term and multi-stage precipitation process enables researchers to flexibly carry out elemental doping. For instance, Shiyou Li *et al.* demonstrated the successful incorporation of magnesium into both transition-metal and lithium sublattices *via* a two-stage precipitation and lithiation sequence.[46] Similarly, Jiantao Wang *et al.* designed a boron-doping protocol that achieved uniform elemental distribution and notable performance improvements through coprecipitation.[47] The sol–gel method (Fig. 3b) provides an alternative route that relies on the hydrolysis and condensation of metal alkoxides or inorganic salts to form a stable sol. The sol is subsequently dried and heat-treated to produce the target material. The method allows for excellent compositional control, especially in multicomponent systems, and enables the preparation of thin films, powders, and coated particles. However, the formation of SC products using sol–gel processing often requires high-temperature sintering and extended calcination times. To further improve uniformity and particle dispersion, researchers have employed mechanical techniques such as long-duration ball milling or manual grinding of dried gels. For example, Yujiang Wang *et al.* utilized a modified sol–gel process involving controlled drying, grinding, and a two-step thermal treatment to promote crystallization while minimizing particle aggregation.[48] Despite these improvements, the total heat treatment time typically exceeds 24 hours, leading to considerable energy consumption and limiting large-scale viability. Molten-salt synthesis (Fig. 3c) offers a promising alternative by using low-melting-point salts to facilitate diffusion and crystal growth. This method simplifies the reaction environment, avoids the formation of undesired secondary phases, and improves both particle size control and phase purity. Haoshen Zhou *et al.* reported that tuning the calcination duration enabled precise control of particle diameter, with an optimized sample reaching a D_{50} value of approximately 413 nanometers.[49] At lower temperatures, solid-state reactions can still occur, but the diffusion rates of atoms (such as Li, Mn, Co, Ni, O, *etc.*) are relatively slow. This tends to promote the formation of numerous fine crystal nuclei, which grow individually and eventually aggregate into polycrystalline particles composed of many small grains, forming "secondary spheres". To obtain a complete single crystal without internal grain boundaries, atoms must possess sufficient energy for long-range ordered diffusion, allowing crystal nuclei to grow continuously and steadily rather than forming new nuclei repeatedly. High temperatures provide this energy, significantly accelerating the bulk diffusion rate of atoms, thereby enabling one or a few nuclei to grow preferentially and ultimately form single-crystal particles with controllable sizes. Therefore, most SC synthesis requires calcination temperatures above 900 °C, and the resulting particles often fall short of the micron scale, thus limiting their structural robustness in full-cell applications. In summary, although traditional methods have been progressively optimized, they still face inherent trade-offs between process complexity, particle size, and structural quality.

To overcome the limitations of traditional methods, recent investigations have focused on developing novel synthesis techniques that can deliver large, structurally intact SC while reducing energy consumption and simplifying process steps. Among these, the self-combustion method (Fig. 3d) presents a low-cost, environmentally friendly approach that relies on redox-driven exothermic reactions between metal nitrates and organic fuels to produce oxide particles without the need for

external heating.[50] This method significantly reduces equipment requirements and simplifies the synthesis protocol. However, the resultant particles typically remain small, approximately 300 nanometers in size, which limits their practical application in commercial battery systems that demand higher mechanical and electrochemical stability. In light of this, Ju Li *et al.* introduced a planetary centrifugal deagglomeration method (Fig. 3e) that utilizes eutectic salt mediation

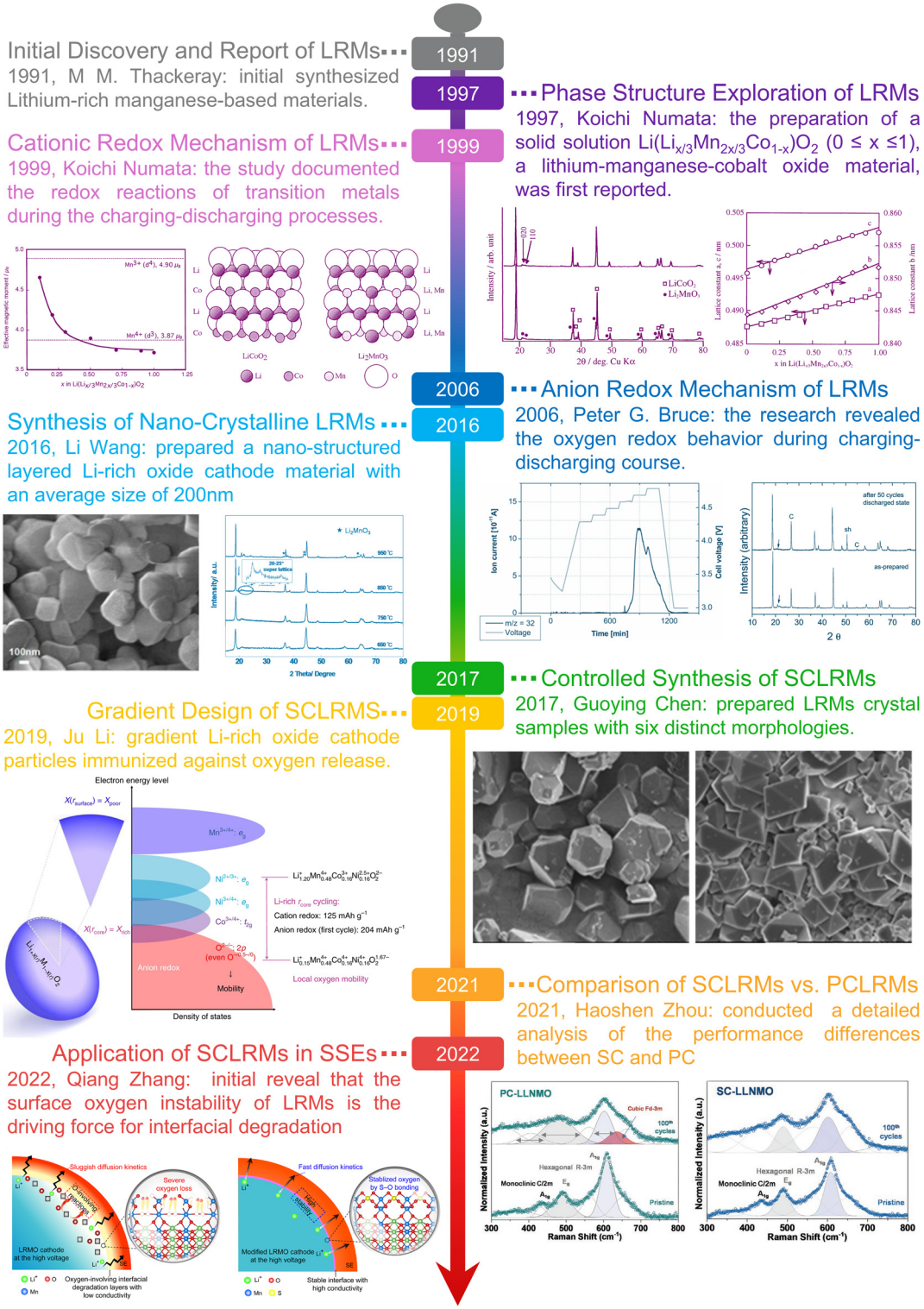

Fig. 2 A brief timeline of LRM development. Copyright 1997 CSJ, 1999 Elsevier, 2006 ACS, 2016 MDPI, 2017 Wiley-ACH, 2019 NPG, 2021 Wiley-VCH, 2022 AAAS.

to promote reactive wetting under moderate mechanical agitation.[51] During processing, transient eutectic salts are melted *in situ*, generating a well-dispersed suspension of metal oxides in liquefied lithium salts. This configuration facilitates the repacking of crystallites and the homogenization of Li^+ distribution throughout the matrix. Upon subsequent calcination, micron-scale SCs with uniform morphology and improved electrochemical properties are obtained. Despite these advantages, the method involves intricate synthesis steps and requires calcination times exceeding 24 hours, which complicate scalability and raise questions about industrial feasibility. In practice, PCLRMs retain their popularity due to lower production costs and simpler processing conditions, such as faster nucleation rates and lower sintering temperatures. However, their inherent grain boundaries and weaker mechanical cohesion can accelerate performance degradation under high-voltage cycling. In contrast, the fabrication of SC materials with better performance often requires elevated synthesis temperatures, slow heating and cooling rates, and prolonged annealing durations to suppress PC phase formation and promote monolithic grain growth. These conditions can inadvertently induce cation disorder or oxygen loss, presenting further challenges for maintaining structural integrity. Therefore, a fundamental trade-off persists between the precision required for high-quality SC formation and the practical need for cost-effective, time-efficient, and scalable manufacturing. Efforts to resolve this tension have shifted toward the design of hybrid or assisted synthesis strategies, such as flux-assisted sintering, microwave-assisted heating, and precursor engineering to reduce lattice defects and enhance grain growth kinetics. In parallel, researchers are also developing scalable reactor designs and process automation protocols to minimize batch-to-batch variability and improve yield. Ultimately, the synthesis pathway plays a decisive role in dictating the final crystal structure, defect concentration, and electrochemical response of SCLRMs. In conclusion, the evolution of synthesis strategies for SCLRMs reflects a shift from complex, energy-intensive routes toward more sustainable, industrially compatible processes. Moving forward, the development of SCLRM synthesis methods must prioritize simplified process design, energy efficiency, and scalability.

3. Physicochemical characteristics and electrochemical behaviors

To clarify the structural differences between PCLRMs and their SC counterparts, a range of morphological and crystallographic analyses were performed. As shown in Fig. 4a and e, the synthesis of SCLRMs requires higher calcination temperatures, prolonged durations, and more precise conditions compared to PCLRMs. PCLRM particles are typically composed of 100–200 nm primary crystallites (Fig. 4d) agglomerated into micron-sized secondary particles (Fig. 4b), forming porous architectures with numerous grain boundaries (Fig. 4c).[52–54] These grain interfaces not only increase the specific surface area but also act as mechanical weak points, facilitating Li^+ diffusion anisotropy, stress accumulation, microcrack formation, and oxygen evolution during cycling. In contrast, SCLRM particles consist of dense, monolithic grains (0.5–2 μm) with smooth surfaces and homogeneously distributed TM (Mn, Ni, and Co), as illustrated in Fig. 4f–h.[55–57] The absence of grain boundaries improves mechanical robustness and electrochemical stability by eliminating structural discontinuities and minimizing internal stress. High-resolution transmission electron microscopy (HRTEM) provides further confirmation: the PCLRM sample (Fig. 4i) displays lattice fringes with ~0.474 nm spacing, corresponding to the (003) plane. In contrast, SCLRMs (Fig. 4j) exhibit an expanded spacing of ~0.482 nm for the (003) plane. The lattice broadening in SCLRMs facilitates rapid Li^+ transport and enhances intrinsic activity. During charging and discharging, the intercalation and deintercalation of Li^+ cause the electrode material's lattice to expand and contract. A larger interlayer spacing provides a buffer zone for this volume change, effectively mitigating the associated stress and thus preserving the structural integrity of the material over extended cycling. This results in a slower capacity decay. Furthermore, a greater lattice spacing facilitates the de-solvation process, which lowers the energy barrier at the interface and reduces the internal battery resistance. It also aids in accommodating larger ions, making SC materials ideal hosts for cationic or anionic doping. However, the long transmission path caused by the intrinsic structure of an SC is disadvantageous. Consequently, it is essential to enhance the lithium-ion transport rate to counteract the limitations posed by long diffusion paths. It also improves mechanical resilience by raising the elastic modulus and delaying phase transitions. Thermal stability is evident in Fig. 4k, which shows significantly less TM dissolution from SCLRM-based cells after two weeks of storage at 60 °C compared to PCLRMs.[51] The shorter Mn–O bonds and higher lattice oxygen activity in PCLRMs make it more susceptible to oxygen release and structural collapse. In contrast, the compact, defect-suppressed SCLRM lattice mitigates such degradation. These structural advantages highlight the superiority of SCLRMs for high-energy, thermally stable Li^+ batteries.

Despite their structural advantages, the preparation of SCLRMs poses challenges in particle size uniformity and morphology control. As depicted in Fig. 4e, extended high-temperature calcination often results in excessive grain growth and broad particle size distribution (*e.g.*, $D_{50} \geq 2000$ nm), akin to an oversintering phenomenon. This heterogeneity leads to electrochemical inconsistencies: large SCLRM particles tend to suffer from incomplete delithiation due to low surface reactivity, while smaller ones are more prone to overcharging and mechanical fracture from drastic volume changes. Moreover, during slurry casting and electrode fabrication, particle size disparity causes large particles to sediment and small particles to agglomerate, resulting in uneven electrode thickness and composition (Fig. 4l), which in turn increases internal resistance and cell-to-cell variability.[49] Specific surface area also

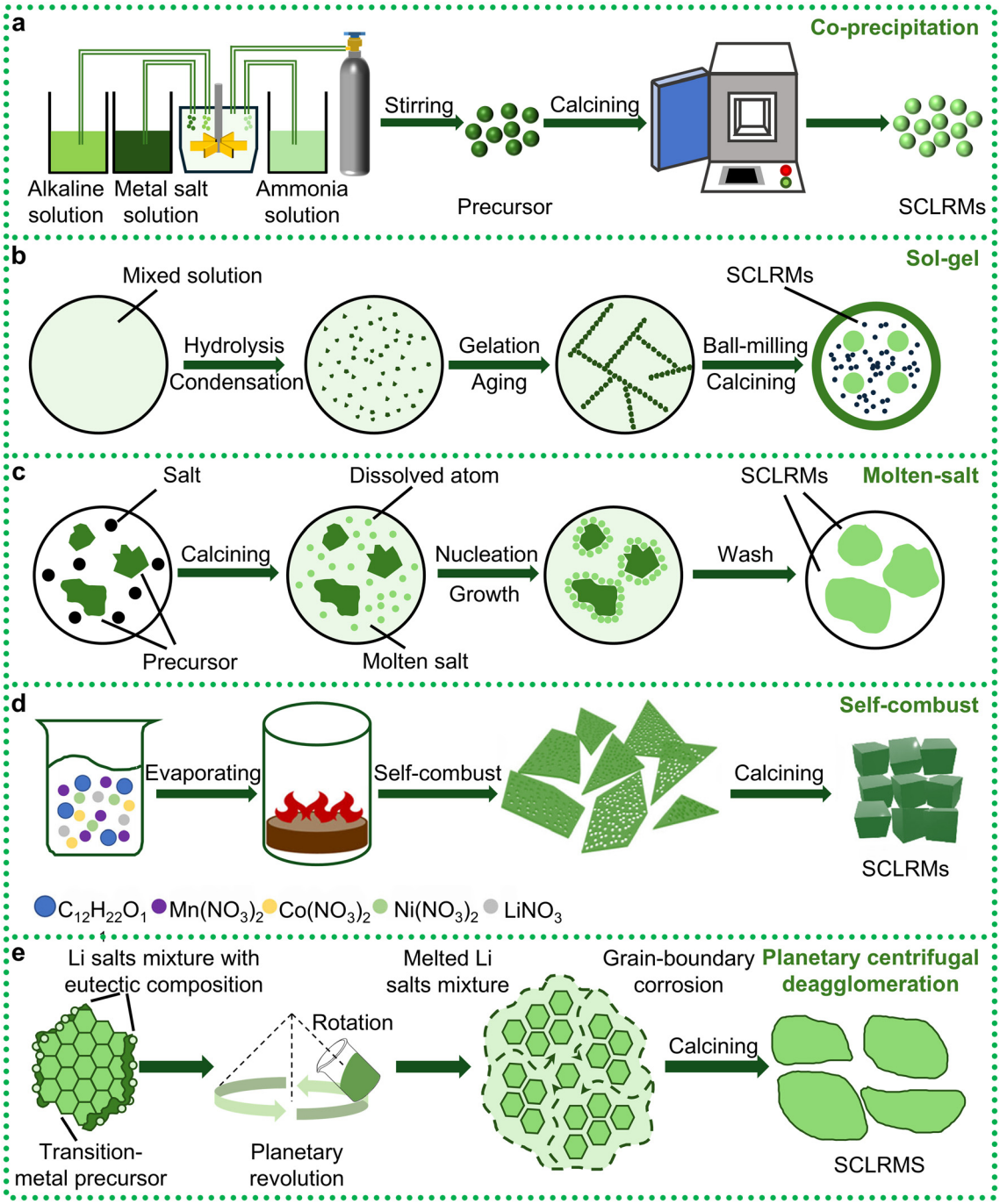

Fig. 3 Different synthesis of LRMs. (a) Co-precipitation. (b) Sol–gel. (c) Molten salt. (d) Self-combustion. Reproduced from ref. 50, copyright 2022 NFSOC. (e) Eutectic salt-assisted planetary centrifugal deagglomeration. Reproduced from ref. 51, copyright 2023 NPG.

plays a critical role. While traditional PCLRMs' design prioritizes high BET surface areas to enhance reaction kinetics, SCLRM materials benefit from lower surface areas that suppress side reactions. For example, Jaephil Cho *et al.* reported submicron SCLRMs with a BET surface area of only 1.5 $m^2\ g^{-1}$ (Fig. 4m), achieving a high tap density of 3.2 $g\ cm^{-3}$ and improved electrode compactness.[60] Although PCLRM particles with high surface areas can deliver high specific capacities, their practical volumetric energy densities (~2400 Wh L^{-1}) and interfacial stabilities remain inferior. Micron-scale SCLRMs with even lower BET values (~0.824 $m^2\ g^{-1}$) offer a favorable balance between structural stability, energy density, and manufacturability.[51] A high BET surface area typically indicates smaller particles, rougher surfaces with more cracks and pores, or a porous structure. At the same time, smaller particles and a higher specific surface area can theoretically

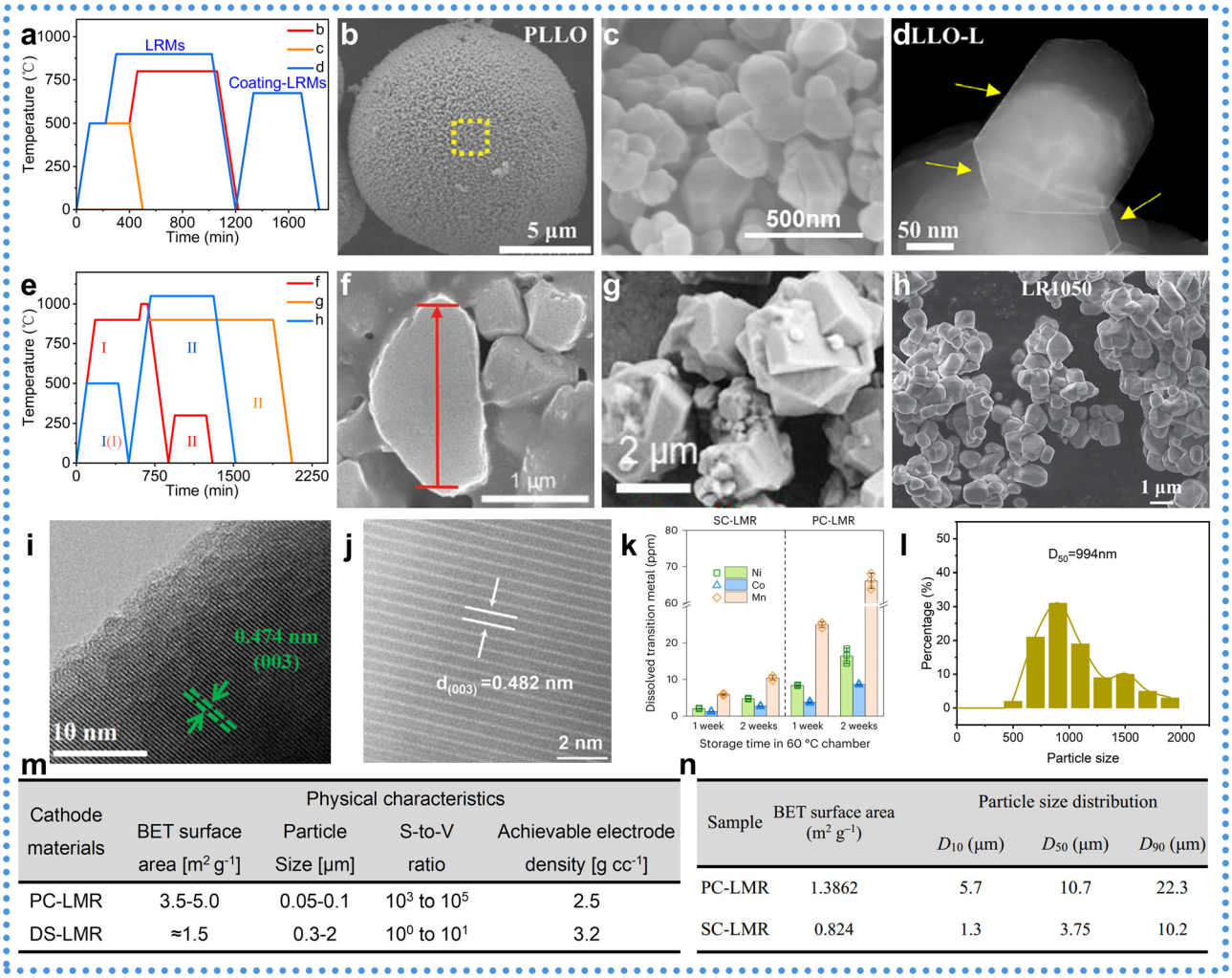

m

Cathode materials	Physical characteristics			
	BET surface area [$m^2 g^{-1}$]	Particle Size [μm]	S-to-V ratio	Achievable electrode density [g cc^{-1}]
PC-LMR	3.5-5.0	0.05-0.1	10^3 to 10^5	2.5
DS-LMR	≈1.5	0.3-2	10^0 to 10^1	3.2

n

Sample	BET surface area ($m^2 g^{-1}$)	Particle size distribution		
		D_{10} (μm)	D_{50} (μm)	D_{90} (μm)
PC-LMR	1.3862	5.7	10.7	22.3
SC-LMR	0.824	1.3	3.75	10.2

Fig. 4 Distinctions of physical properties between SCLRMs *versus* PCLRMs. (a) The calcination temperature curve for the preparation of PCLRMs. Data are from ref. 52–54. (b)–(d) SEM patterns of PCLRMs. Reproduced from ref. 52–54, copyright 2023 Wiley-VCH, 2024 Elsevier, 2025 Wiley-VCH. (e) The calcination temperature curve for the preparation of SCLRMs. Data are from ref. 55–57. (f)–(h) SEM patterns of SCLRMs. Reproduced from ref. 55–57, 2022 Wiley-VCH, 2023 Elsevier, 2024 ACS. (i) and (j) TEM patterns of PCLRMs and SCLRMs. Reproduced from ref. 58 and 59, copyright 2024 Elsevier and 2024 Wiley-VCH. (k) Dissolved Ni, Co and Mn in the electrolytes measured using an ICP optical emission spectrometer after one and two weeks of storage at 60 °C. Reproduced from ref. 51, copyright 2023 NPG. (l) Grain size distribution of SCLRMs. Reproduced from ref. 49, copyright 2023 RSC. (m) and (n) A comparison of physical characteristics of submicron-sized SCLRMs and micron-sized SCLRMs with PCLRMs. Reproduced from ref. 60 and 51, copyright 2021 Wiley-VCH and 2023 NPG.

shorten the Li^+ diffusion path and are beneficial for rate capability. However, this comes with a critical drawback: it increases the contact area between the electrode material and the electrolyte. The surface of LRMs is highly chemically active, and contact with the electrolyte triggers persistent and detrimental side reactions. A larger contact area provides more reactive sites, thereby exacerbating the dissolution of transition metal ions, the release of lattice oxygen, interface instability, continuous oxidative decomposition of the electrolyte, and the accumulation of byproducts. Due to the superior overall structure of SCs, they are free from pores compared to their PC counterparts. As shown in the BET results in Fig. 4m and n, the SC structure reduces the specific surface area, significantly minimizing sites prone to side reactions. This further enhances the structural stability and safety of SCs during charge and discharge processes. Consequently, the development focus has shifted from sub-200 nm SCLRMs toward optimized micron-sized particles.

Variations in the physical properties result in significantly different electrochemical performance (Table. 1). The electrochemical performance of LRM cathode materials is closely associated with their structural form, particularly in the comparison between the morphologies of SCLRMs and PCLRMs. One key distinction lies in gas evolution behavior, especially under high-voltage conditions where oxygen redox processes and side reactions dominate. As shown in galvanostatic charge/discharge tests at 40 mA g^{-1} (Fig. 5a), both PCLRMs and SCLRMs exhibit typical voltage plateaus linked to lattice

Table 1 Comparison of typical single crystal properties

Sample name	Capacity	Capacity retention	Rate performance
$Li_{1.2}Ni_{0.2}Mn_{0.6}O_2$ [43]	257 mAh g^{-1} at 20 mA g^{-1}	94% after 200 cycles at 1C	197 mAh g^{-1} at 1C
SCL-10h [49]	258 mAh g^{-1} at 25 mA g^{-1}	97.3% after 250 cycles at 1C	160 mAh g^{-1} at 5C
SC-LMR [51]	259 mAh g^{-1} at 25 mA g^{-1}	90.6% after 100 cycles at 1C	
GSC-LLO [55]	260 mAh g^{-1} at 20 mA g^{-1}	97.6% after 100 cycles at 1C	
SC-HBLR [59]	236.26 mAh g^{-1} at 25 mA g^{-1}	87.42% after 300 cycles at 1C	144.9 mAh g^{-1} at 5C
NAS-LMNCO [63]	270 mAh g^{-1} at 25 mA g^{-1}	94.6% after 200 cycles at 1C	136.7 mAh g^{-1} at 5C
TSC-LNCM [64]	296.3 mAh g^{-1} at 25 mA g^{-1}	90.7% after 400 cycles at 1C	183.6 mAh g^{-1} at 3C
LLO@PPA [65]	245 mAh g^{-1} at 20 mA g^{-1}	89.15% after 300 cycles at 0.5C	124 mAh g^{-1} at 4C
DL-LLO [66]	302.6 mAh g^{-1} at 25 mA g^{-1}	82.5% after 300 cycles at 1C	150 mAh g^{-1} at 5C
MZCN-LMR [67]	305 mAh g^{-1} at 20 mA g^{-1}	80.5% after 500 cycles at 1C	211 mAh g^{-1} at 5C

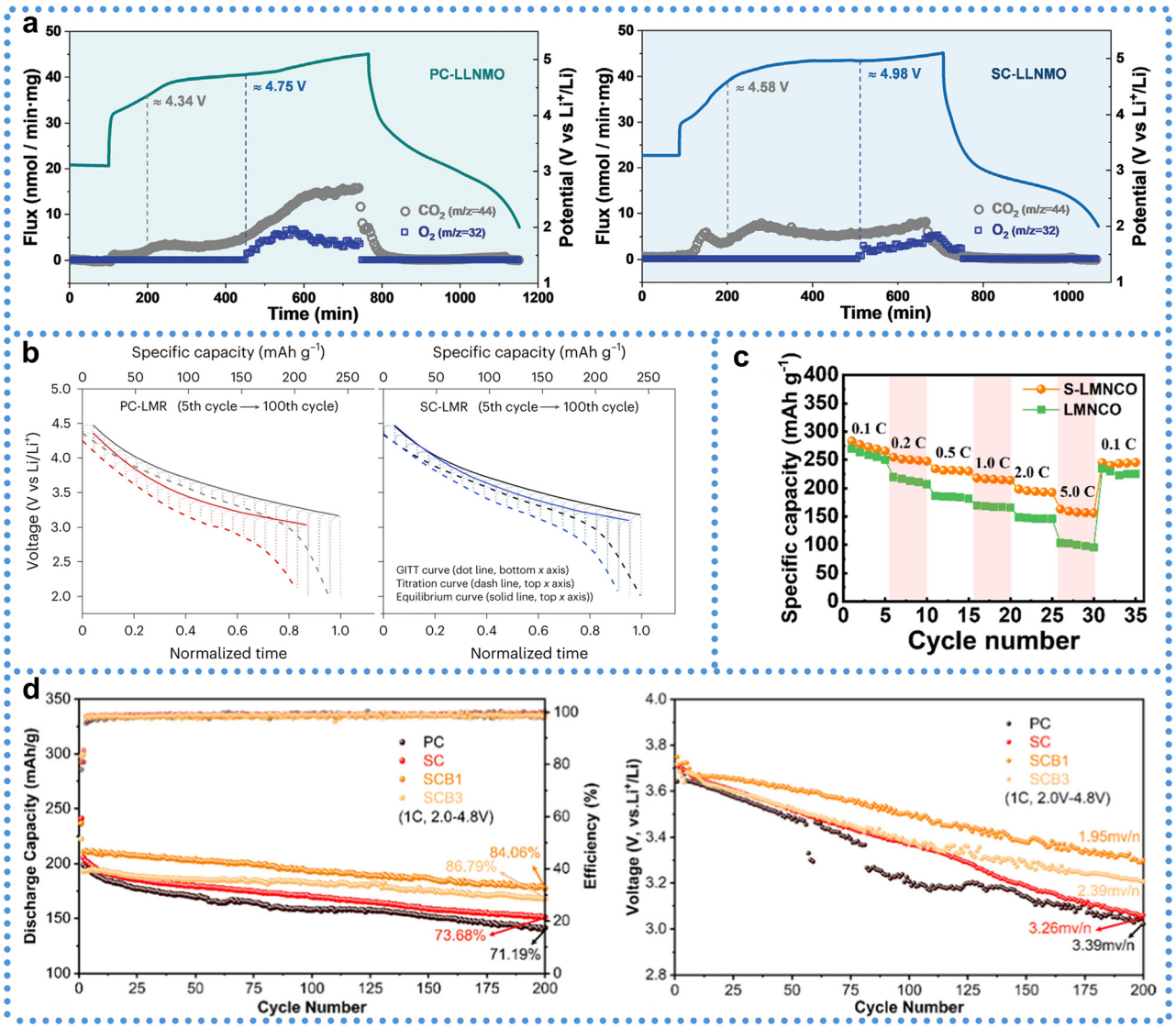

Fig. 5 Electrochemical performance comparison between SCLRMs and PCLRMs. (a) Gas evolution profiles of CO_2 (m/z = 44) and O_2 (m/z = 32). Reproduced from ref. 43, copyright 2021 Wiley-VCH. (b) Discharge curves of GITT. Reproduced from ref. 51, copyright 2023 NPG. (c) Rate capability. Reproduced from ref. 61, copyright 2024 Elsevier. (d) Cycling performances and average voltage profiles. Reproduced from ref. 62, copyright 2024 ACS.

oxygen activation.[43] However, gas chromatography–mass spectrometry (GC-MS) reveals that oxygen release in PCLRMs begins at approximately 4.7 V and intensifies above 5.0 V. In contrast, SCLRMs delay oxygen evolution to around 4.98 V and show reduced overall release intensity. This may be attributed to the more compact and coherent lattice structure of

SCLRMs, which restricts oxygen channel formation and stabilizes the lattice under deep delithiation. In addition to oxygen, CO_2 evolution provides insight into interfacial reactivity. GC-MS identifies two CO_2 generation regimes: the first above ~4.34 V corresponds to the decomposition of surface Li_2CO_3, while the second above ~4.6 V is associated with electrolyte degradation, potentially catalyzed by surface TM or reactive oxygen species. Although both PCLRMs and SCLRMs release CO_2 in these regions, the SC samples consistently show lower gas intensities. This can be linked to their lower BET surface area and reduced density of high-energy surface sites. The suppression of parasitic gas evolution in SCLRMs indicates a more restrained interfacial environment, which may enhance long-term stability and safety in full-cell operation. Beyond gas behavior, rate capability is another key differentiator. As demonstrated in Fig. 5b and c, SCLRMs show superior capacity retention across increasing current densities.[51,61] This is closely tied to the transport pathways within each material. In PCLRMs, grain boundaries act as discontinuities that impede Li^+ mobility. These boundaries are often regions of atomic disorder and defect accumulation, creating local energy barriers for ion transport and electron conduction. Furthermore, the random orientation of grains forces Li^+ to traverse a variety of crystallographic directions, many of which are less favorable than the high-mobility (003) plane. By contrast, the continuous lattice of SCLRMs supports aligned ion transport and eliminates the need to cross grain boundaries, reducing ionic resistance and improving rate performance. Moreover, the absence of structural mismatches between grains minimizes electronic scattering and voltage polarization under high-rate conditions. However, it is important to acknowledge that real-world rate performance also depends on other factors, such as particle size, electrode formulation, and electrolyte–electrode compatibility. While SCLRMs tend to outperform PCLRMs under controlled test conditions, the absolute advantage can vary depending on these parameters. Nevertheless, the intrinsic structural continuity of SCLRMs offers a clear benefit in terms of kinetic facilitation and interfacial stability, particularly under aggressive electrochemical environments.

Long-term cycling performance and voltage retention are crucial parameters for evaluating the durability of LRM cathodes. Differences between SC and PC forms are particularly evident over extended charge/discharge cycles. In PCLRMs, the presence of grain boundaries often leads to mechanical and electrochemical degradation. These intergranular regions act as stress concentrators during repeated lithiation and delithiation, promoting microcrack initiation and propagation. Cracks expose fresh surfaces to the electrolyte, accelerating side reactions such as TM dissolution and cathode–electrolyte interphase (CEI) instability.[62] These processes contribute to impedance growth, voltage hysteresis, and capacity fading. In contrast, the absence of grain boundaries in SCLRMs provides a structurally unified framework that can better accommodate volume changes and suppress localized mechanical failure. As shown in galvanostatic intermittent titration technique (GITT) results (Fig. 5b), SCLRMs maintain the shape of its voltage curve more effectively than PCLRMs over 100 cycles, indicating lower structural distortion and more reversible phase transitions.[51] Quantitatively, SCLRMs exhibit a capacity retention of 86.79%, significantly higher than the 71.19% observed for PCLRMs (Fig. 5d).[68] In terms of voltage stability, the average voltage decay per cycle is also reduced in SCLRMs (1.95 mV per cycle) compared to PCLRMs (3.39 mV per cycle). These differences suggest that the SC morphology helps mitigate both electrochemical and mechanical degradation pathways during long-term operation. The improved voltage retention in SCLRMs may also relate to more uniform CEI formation. In PCLRMs, heterogeneous stress distribution across grains results in non-uniform CEI growth and compositional instability, which amplifies polarization and capacity decay. SCLRMs, by virtue of their smoother surface and lower interfacial reactivity, tend to form a more uniform and stable CEI. This enables better preservation of ionic pathways and electronic contact during extended use. While these advantages are consistent across many studies, it is worth noting that SCLRMs are not entirely immune to aging. Under high-voltage or elevated-temperature cycling, even SC particles may develop surface cracks or partial oxygen loss, particularly at edges or pre-existing defect sites. These subtle forms of degradation, although less frequent than in PCLRMs, can still affect performance over long durations. Moreover, performance outcomes are influenced not only by crystallinity but also by factors such as particle size distribution, porosity, electrode density, and electrolyte formulation. Although SCLRMs have demonstrated improved cycling durability and voltage retention under controlled laboratory conditions, these advantages are not universally guaranteed across all practical applications. The contribution of grain-boundary elimination to long-term stability may vary depending on synthesis consistency, electrode architecture, and cell integration. Therefore, while SCLRMs exhibit certain benefits in structural integrity and interfacial behavior compared to PCLRMs, these findings require further validation across diverse testing environments. The actual capacity of SCLRMs remains below the theoretical limit (~350 mAh g^{-1}), indicating the need for further improvements.

4. Strategies to mitigate degradations

To address persistent challenges such as voltage decay, structural degradation, and interfacial instability in SCLRMs, ion doping has emerged as a practical and effective modification strategy (Fig. 6a). By introducing heteroatoms into specific crystallographic sites, doping improves lattice stability, enhances Li^+ diffusion, suppresses oxygen release, and prolongs cycling life. Although this approach is well established for PC counterparts, its application in SCLRMs is still underdeveloped due to the complexity of SC synthesis. Nevertheless, successful strategies in PC systems are highly relevant and transferrable to SC materials. Doping at Li sites, TM sites, or oxygen sites allows targeted control over structural and electronic properties, while multi-site co-doping is increasingly

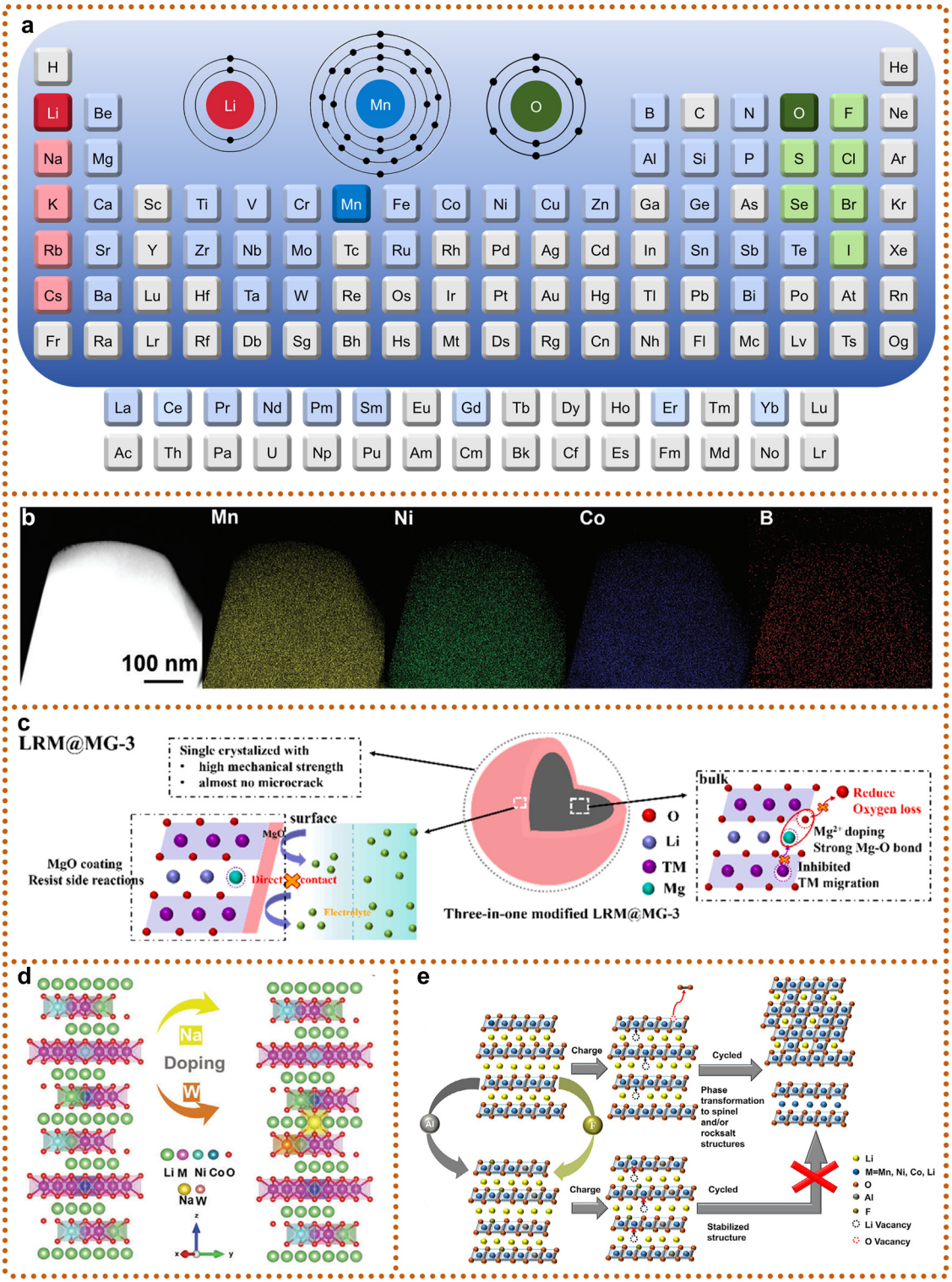

Fig. 6 Typical doping strategies for SCLRMs. (a) Schematic of representative doping sites and heteroatomic doping summary of LRMs. (b) TM site doping of SCLRMs represented by B-doping. Reproduced from ref. 59, copyright 2024 Wiley-VCH. (c) Li site and TM site doping of SCLRMs represented by Mg-doping. Reproduced from ref. 67, copyright 2025 Elsevier. (d) and (e) Multi-site co-doping of SCLRMs represented by Na, W-doping and F, Al-doping. Reproduced from ref. 69 and 70, copyright 2023 Wiley-VCH and 2025 Wiley-VCH.

used to generate synergistic improvements. Among monatomic dopants, boron (B) has attracted considerable attention due to its small ionic radius and high bond energy with oxygen. B atoms can reside in interstitial regions between TM and O atoms, forming strong B–O covalent bonds that enhance lattice oxygen stability.[71] Zhian Zhang *et al.* employed a boric acid treatment to introduce both gradient B doping and a spinel-like $Li_2B_4O_7$ surface layer (Fig. 6b).[59] This dual modification strategy minimized grain boundaries, mitigated mechanical strain, and enabled reversible anion redox, while also expanding interlayer spacing and improving Li^+ transport. Magnesium (Mg) doping provides another example of dual-function modification. Shiyou Li *et al.* used $MgCO_3$ to assist in crystallization and simultaneously form a protective MgO coating, eliminating post-synthesis washing (Fig. 6c).[72] Mg^{2+} can substitute both Li and TM sites, depending on the synthesis conditions. When occupying Li sites, Mg strengthens Mg–O bonding, inhibiting oxygen evolution. When substituting TM sites, Mg reduces Mn–O covalency, suppressing the formation of electron holes in O_{2p} orbitals and preventing oxygen overoxidation. These mechanisms highlight the importance of understanding dopant site preferences, particularly for elements capable of multiple substitutions. Despite these advances, most studies continue to focus on single-site substitution. Research on applying single-element doping across multiple sites remains limited, and few works compare site-specific effects systematically. As structural control and compositional complexity increase, the rational design of dopants for SCLRMs will require deeper insight into the relationships between atomic site occupation, local bonding environments, and electrochemical performance.

As performance requirements for Li^+ batteries increase, the limitations of single-element doping in SCLRMs have become apparent, motivating a shift toward co-doping strategies involving two or more dopants. These approaches leverage the complementary properties of multiple elements to enhance lattice stability, suppress oxygen release, improve conductivity, and extend cycle life. A representative example is the Na–W co-doping strategy (Fig. 6d) developed by Hao Liu *et al.*[69] In this design, sodium ions substitute Li sites to expand interlayer spacing and reinforce the layered structure, while tungsten ions preferentially occupy TM sites, enhancing mechanical robustness and reducing cation mixing. The oxygen vacancy formation energy increased from 6.75 eV in the pristine material to 9.26 eV in the co-doped system, indicating significantly improved oxygen stability. Additional benefits included enhanced cation ordering, a higher $I(003)/I(104)$ intensity ratio, and growth of larger SCs, all contributing to improved long-term performance. More advanced strategies involve simultaneous doping with both cations and anions, allowing for charge compensation and electronic structure tuning. For example, Bao Wang *et al.* introduced a co-doping system using fluorine (F^-) and aluminum (Al^{3+}), as shown in Fig. 6e.[70] The strong Al–O bonds improved structural integrity and increased the energy barrier for oxygen release. Concurrently, F^- replaced oxygen in the lattice, reducing oxygen gas evolution and suppressing parasitic reactions between the cathode and the electrolyte. Additionally, F incorporation increased the diffusion barrier for TM ions, limiting their migration and improving interface stability.[73] These combined effects demonstrate the potential of co-doping to manipulate both conduction and valence bands, optimize the bandgap, and improve redox reversibility. Despite promising results, challenges remain in fully understanding and optimizing co-doping strategies. While advanced techniques such as scanning transmission electron microscopy and X-ray absorption spectroscopy have clarified dopant positions and bonding configurations, the cooperative effects between different elements are still not well understood. Furthermore, theoretical studies suggest that the co-segregation of isovalent dopants may induce grain boundary phase transformations toward spinel or olivine structures, which could improve cycling stability.[74] However, this hypothesis has yet to be validated experimentally in SCLRMs. Future work should combine atomistic modeling, high-throughput screening, and *in situ* characterization to establish clear design rules for multi-element and multi-site doping.

Following progress in lattice doping strategies, surface-level modifications have emerged as a complementary and essential pathway to further enhance the structural integrity and electrochemical performance of SCLRMs. In contrast to bulk-phase regulation, surface engineering directly targets interfacial reactions, aiming to suppress parasitic decomposition, stabilize the electrode–electrolyte interface, and mitigate phase transitions during extended cycling, especially under high-voltage operation. Among the surface engineering techniques, inorganic coating has gained significant attention due to its effectiveness in mitigating structural degradation and improving long-term cycling stability. Conventional coatings such as Na_2WO_4, $Li_2B_4O_7$, and Li_3PO_4 are applied *ex situ* to form protective barriers. However, due to poor lattice matching with the single-crystal host, these layers often delaminate during cycling, accelerating performance decay. To overcome this limitation, spinel-type $Li_4Mn_5O_{12}$ coatings have been introduced. Their structural compatibility and three-dimensional lithium diffusion paths make them ideal for *in situ* growth on the SCLRM surface. Zhaozhe Yu *et al.* constructed a dual-structured surface design featuring an Al^{3+}-doped spinel layer and a gradient-doped layered subsurface, significantly enhancing interface stability while mitigating oxygen release and electrolyte corrosion (Fig. 7a).[63] This architecture improved both capacity retention and long-term durability. Similarly, Xianyou Wang *et al.* applied a 5 nm $Li_4Mn_5O_{12}$ coating *in situ* and observed reduced (003) peak shifts in XRD analysis after repeated cycling, suggesting suppression of irreversible phase transitions (Fig. 7b).[64] The resulting cathode achieved an initial discharge capacity of 296.4 mAh g^{-1} at 0.1C and retained 97.4% capacity after 300 cycles at 1C.

To further expand the functionality of surface modifications, dual-layer (DL) and hybrid coatings have emerged as a practical solution to integrate mechanical compliance and chemical robustness. Polymer-based coatings offer exceptional flexibility and can self-accommodate local strain or micro-

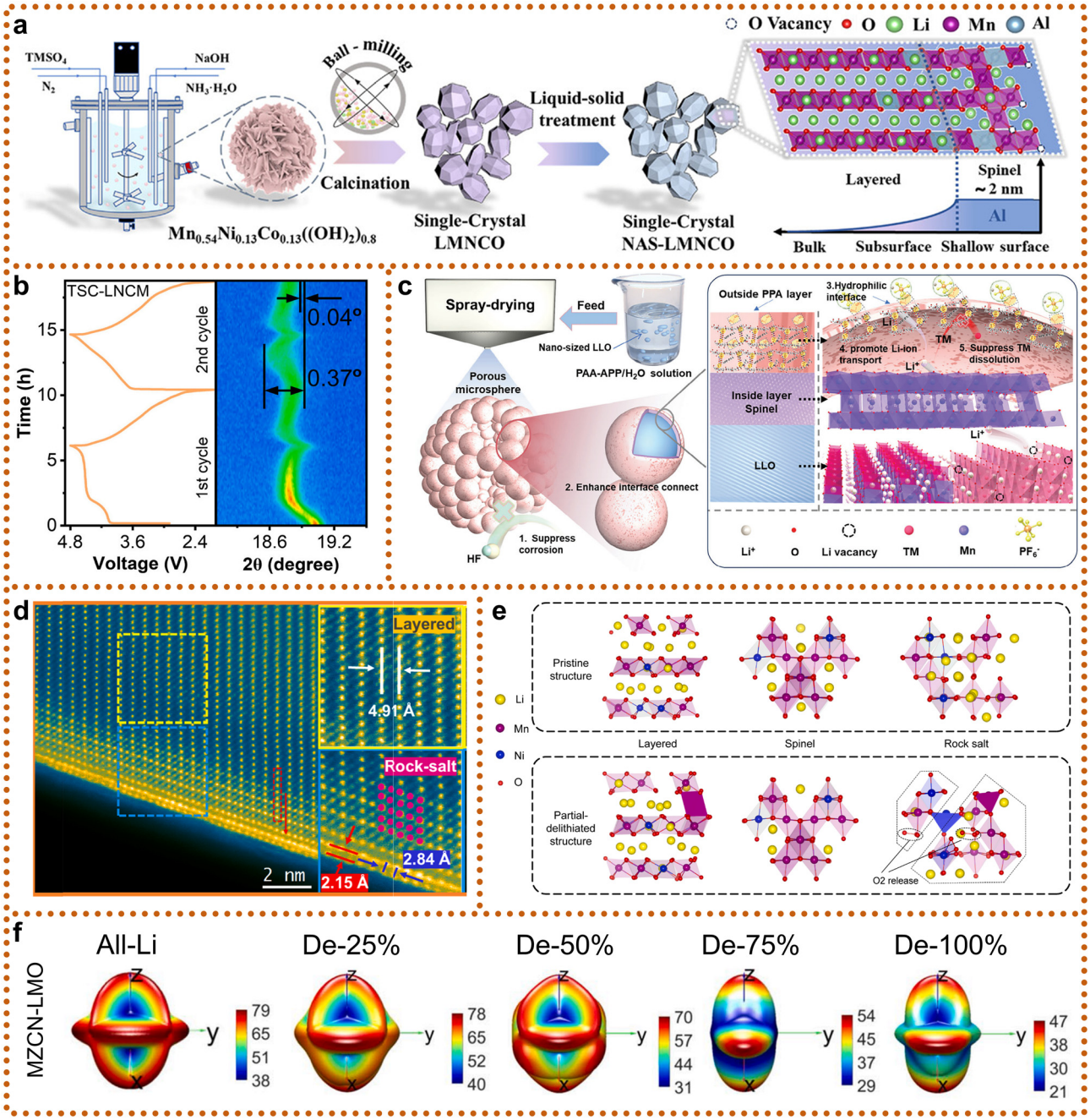

Fig. 7 Surface modification strategy of SCLRMs. (a) and (b) Single layer coating represented by spinel coating. Reproduced from ref. 72 and 64, copyright 2024 Wiley-VCH and 2023 Elsevier. (c)–(e) DL coating represented by PPA and spinel coating, $LiGdO_2$ and rock-salt coating, and Li_3PO_4 rock-salt outer layer with a spinel inner layer. Reproduced from ref. 65, 66, 75, copyright 2024 Wiley-VCH, 2022 Elsevier, and 2024 Elsevier. (f) High entropy surface engineering. Reproduced from ref. 67, copyright 2024 Elsevier.

cracks during cycling, while inorganic components such as oxides improve mechanical hardness and thermal stability. Jinlong Yang *et al.* developed an *in situ* polymer–inorganic hybrid coating using polyacrylic acid and ammonium polyphosphate as precursors to form a crosslinked polypropylene phosphate amide (PPA) layer on Li-rich oxide nanoparticles (Fig. 7c).[65] The spray-drying method facilitated uniform encapsulation and led to the spontaneous formation of a secondary spinel phase at the surface. This structure improved electrolyte wettability, mitigated surface side reactions, and enhanced lithium-ion transport, collectively leading to improved capacity retention and rate performance. However, the relatively low thermal stability of polymer layers, generally degrading above 250 °C, restricts their use in high-temperature applications. To address these limitations, Hao Liu *et al.* introduced a nanometer-scale epitaxial rock salt NiO coating doped with Gd and

an atomically thin $LiGdO_2$ layer to stabilize the single-crystal surface (Fig. 7d).[75] This configuration minimized surface reactivity and achieved 93.4% capacity retention after 500 cycles at 1C. Furthermore, Jinsong Wu *et al.* designed a robust DL cathode–electrolyte interphase (CEI) structure comprising an amorphous Li_3PO_4 outer layer and a disordered spinel $Li_xNi_yMn_{3-x-y}O_4$ inner layer uniformly distributed on the surface of $Li_{1.2}Ni_{0.2}Mn_{0.6}O_2$ particles (Fig. 7e).[66] The coating effectively suppressed the layered-to-spinel-to-rock-salt phase transformation and prevented oxygen release and TM dissolution. As a result, the initial specific capacity was improved from 265 to 302.6 mAh g^{-1}, the coulombic efficiency increased from 82.5% to 90.3%, and the capacity retention after long-term cycling was substantially enhanced. These composite coating strategies offer significant improvements in surface protection, enabling SCLRMs to maintain electrochemical performance under demanding operating conditions.

Beyond conventional protective layers, entropy-driven surface engineering provides an advanced route to regulate the redox behavior and mechanical stability of SCLRMs. By introducing multiple dopant elements into the surface region, a high-entropy environment is formed that alters the local electronic structure and suppresses irreversible degradation. In lithium-rich oxides, lattice oxygen often participates in charge compensation during delithiation, forming unstable $O^{(2-n)-}$ species.[76] These species tend to undergo O–O dimerization, leading to oxygen release, TM migration, and eventual structural collapse from the surface into the bulk. When the coulombic repulsion energy approaches the charge transfer gap, orbital overlap between the O_{2p} and the TM–oxygen antibonding states allows partial electron delocalization, enabling more reversible oxygen redox reactions. Dingguo Xia *et al.* constructed a high-entropy surface on monodisperse $Li_{1.2}Ni_{0.13}Co_{0.13}Mn_{0.54}O_2$ single crystals by doping Mg, Zn, Cu, and Nb (Fig. 7f).[67] Density functional theory calculations revealed that the dopants introduced local electrostatic field disorder, broadened the O_{2p} band, and enhanced hybridization with TM orbitals, thereby stabilizing the oxygen redox process. The doped cathode demonstrated 80.5% capacity retention after 400 cycles and a voltage decay of just 0.7 mV per cycle. This strategy also mitigated lattice strain anisotropy, supporting long-term structural integrity under high-voltage cycling. Therefore, surface engineering strategies including coherent inorganic coatings, dual-layer composite architectures, and entropy-regulated chemical modification collectively provide a comprehensive framework for improving the interfacial and structural stability of monodisperse SCLRMs. However, the complex interaction mechanisms among multiple elements remain unclear and the intricate elemental effects can only be roughly represented through entropy. Future research should focus on understanding the interfacial interactions at the atomic level, optimizing scalable and low-temperature synthesis methods, and integrating these surface modifications into full-cell systems.

Building on the advantages of doping and surface modifications, crystal morphology control offers a complementary strategy to improve the electrochemical and mechanical performance of SCLRMs without introducing foreign elements. By optimizing the morphology, including particle size, surface structure, and internal ordering, Li^+ transport pathways can be streamlined, high-activity crystal planes can be preferentially exposed, lattice strain can be minimized, and compaction density can be enhanced.[77] To maximize the intrinsic properties of materials under spatial constraints, Yuefeng Su *et al.* designed a Kongming-lock morphology (KML), inspired by a traditional Chinese puzzle, comprising interlocked micron-sized plate-like primary particles forming dense secondary architectures (Fig. 8a).[78] This morphology, combined with Li^+/Ni^{2+} intermixing regulation, reduced porosity and significantly increased volumetric energy density, achieving 835 mAh cm^{-3}. KML particles exhibited remarkable lattice stability, with only 1.59% volume change during the first cycle and 96.3% capacity retention after 100 cycles, while the *a*/*b* and *c*-axis deformations offset each other. These results demonstrate that the precise design of local ordering and morphology can effectively mitigate structural degradation. In another study, Haoshen Zhou *et al.* synthesized well-dispersed SCs by tuning the Li/TM ratio during a solid-state reaction, enabling a solid-state exfoliation mechanism that converted agglomerated secondary particles into monodisperse single grains (Fig. 8b).[79] At a Li/TM ratio of 1.575, lithium accumulation occurred at grain boundaries, whereas at 1.8, lithium distribution became more uniform across the particles after calcination at 900 °C. Notably, even after extended heat treatment, lithium diffusion remained dominated by intragranular pathways, influencing both surface and bulk compositions. GPA analysis further confirmed that such modulation led to significantly reduced internal stress and more homogeneous mechanical distribution across SCs (Fig. 8c).[79]

These findings collectively emphasize the importance of crystallographic morphology control in improving both ionic conductivity and mechanical robustness. Morphological design should thus be tailored within spatial constraints of electrode architecture to fully exploit the potential of SCLRMs in practical applications.

In addition to morphology, grain size is a critical parameter influencing ion transport behavior, mechanical stability, and electrode-level packing characteristics of SCLRMs. Early SC cathodes typically exhibit grain sizes of around 200 nm (Fig. 2); such a small size fails to exploit the advantages of SCLRMs and even results in inferior electrochemical performance compared to conventional PCLRMs (<225 mAh g^{-1}). Recent advances have enabled the fabrication of particles exceeding 2 μm in size (Fig. 8d).[51] These larger crystals exhibit near-perfect lattice order (Fig. 8e), effectively eliminating stress concentrators such as grain boundaries and dislocations, thereby achieving superior fracture resistance and thermal creep strength.[51] Their low porosity benefits compaction and helps suppress electrolyte-driven degradation. However, size increase is not universally advantageous. During charge–discharge cycling, micron-scale cathodes (*e.g.*, M-LR, 940 nm) were observed to exhibit high Li^+ concentration gradients

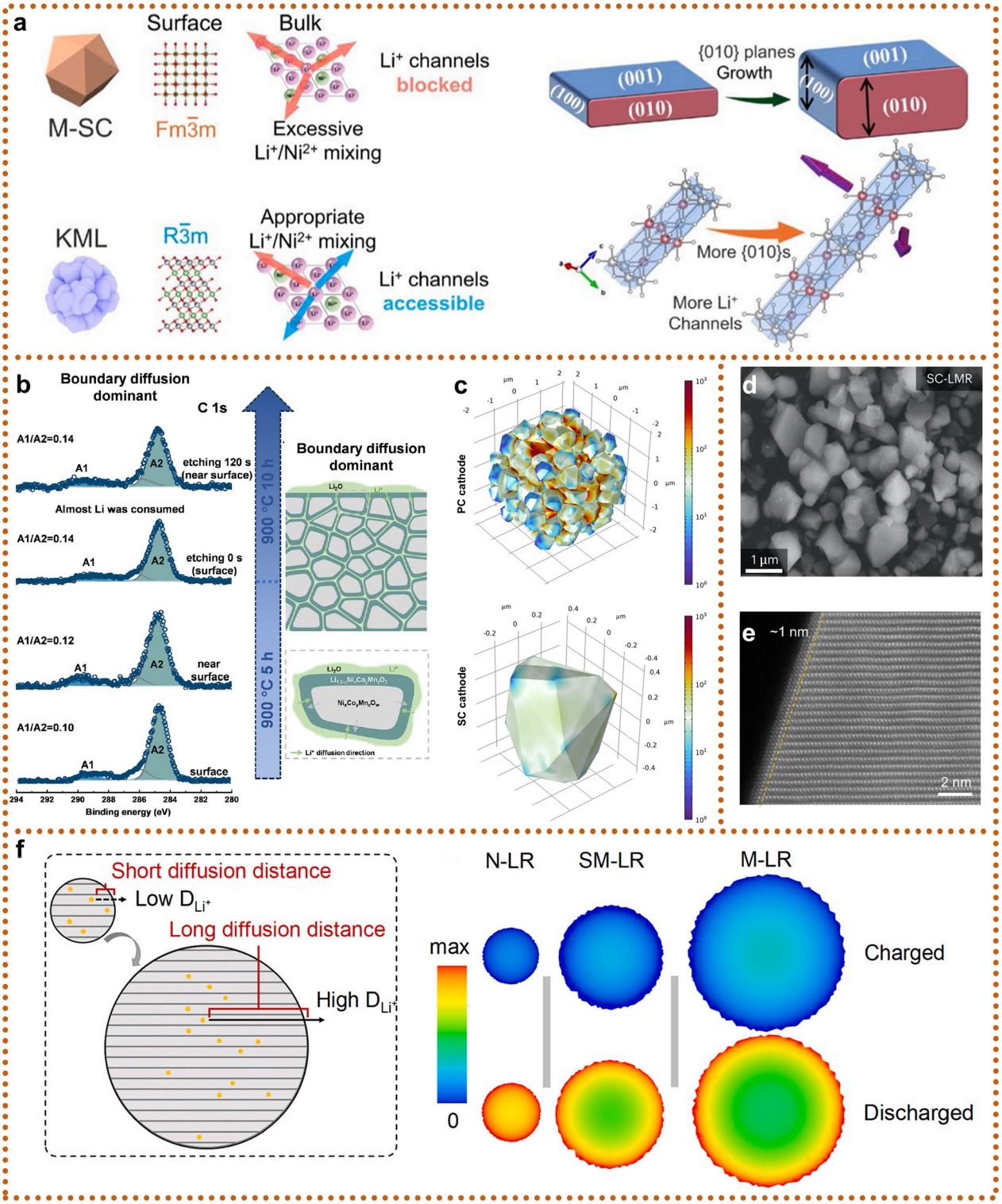

Fig. 8 Crystal architecture engineering of SCLRMs. (a) Crystal morphology regulation. Reproduced from ref. 78, copyright 2025 Elsevier. (b) and (c) Li/TM value modulation and stress distribution. Reproduced from ref. 79, copyright 2025 Elsevier. (d) and (e) Crystal size control. Reproduced from ref. 51, copyright 2023 NPG. (f) Simulation results of Li^+ diffusion in the initial cycle and schematic diagram of the synergistic effect of diffusion coefficient and diffusion distance. Reproduced from ref. 80, copyright 2022 Elsevier.

between the surface and the bulk, as demonstrated by Zhaoping Liu *et al.* (Fig. 8f).[80] This heterogeneity results in localized over-lithiation or under-lithiation, leading to kinetic polarization, volume expansion (up to 5–8%), and microcracking. Such effects degrade ionic conductivity and mechanical integrity, accelerating particle fracture and capacity fading. In contrast, nanosized grains (*e.g.*, N-LR, 101 nm) showed more uniform Li^+ distribution but suffered from lower compaction density and higher reactivity. Optimizing grain size not only involves choosing the appropriate average diameter but also tailoring particle shape, surface structure, and inter-particle connectivity. Looking forward, morphology engineering should be synergistically integrated with compositional and interfacial optimization. Composite strategies combining morphology regulation, surface coating, and lattice doping are anticipated to achieve additive or even multiplicative improvements in performance. Moreover, the coating and sintering processes used to achieve morphology modification can induce surface-layer reconstruction or doping phenomena, which may influence interfacial stability and reaction pathways. Therefore, future studies should pay close attention to these induced effects, with high-resolution characterization and modeling tools used to guide rational design. Such integrated strategies are expected to pave the way for high-performance SCLRMs with optimized morphology, structure, and interfacial compatibility.

5. All-solid-state battery applications

After meticulously designing the morphology and structure of LRMs and systematically exploring how to suppress particle cracking and shorten Li^+ diffusion pathways to enhance intrinsic structural stability, it is natural to shift our focus to their ultimate application scenario—ASSBs. In this device-level system, the pre-engineered high structural integrity and stable interfacial characteristics become key prerequisites for addressing the severe solid–solid interface challenges in ASSBs. However, the unique device structure of ASSB introduces new scientific issues: point-to-point contact between the cathode and solid-state electrolyte, significant interfacial impedance, and stress concentration during charge–discharge processes impose even more stringent demands on the morphology, surface state, and mechanical strength of LRMs. While prior modification strategies for SCLRMs have predominantly focused on mitigating interfacial instability and oxygen loss in liquid electrolyte systems, their applicability in ASSBs demands re-examination. ASSBs eliminate flammable liquid electrolytes and separators by employing solid-state electrolytes (SSEs), enabling compact cell configurations with theoretical energy densities surpassing 700 Wh kg^{-1}. The integration of high-capacity materials, such as lithium metal anodes, along with superior safety and extended lifespan, underscores the transformative potential of ASSBs.[81] Within this context, SCLRMs exhibit structural and mechanical advantages that are particularly compatible with the demands of solid-state systems. Unlike their PC counterparts, which are composed of aggregated primary particles with grain boundaries susceptible to intergranular cracking, SCLRMs consist of a continuous SC domain that minimizes mechanical rupture and preserves structural integrity over extended cycling.[82] The solid–solid interface in ASSBs is not wetted by a liquid medium, thus requiring intimate physical and chemical contact to ensure effective Li^+ transport. Secondary particle cracking in PC-LRMs leads to irreversible loss of contact with SSEs and spatial heterogeneity in current distribution.[83] In contrast, SCLRMs—especially those with reduced particle size—offer shortened lithium diffusion paths and minimize interfacial stress through isotropic ion migration. They also accommodate anisotropic volume expansion more effectively, particularly the *c*-axis elongation and *a*/*b*-axis contraction that occur during initial charge due to oxygen redox activation.[84–86] As visualized in Fig. 9a, repeated cycling, pressing, or mechanical processing leads to the formation of microcracks in PC cathodes, undermining solid–solid contact and increasing interfacial impedance.[82] In comparison, SCLRMs demonstrate enhanced crack resistance due to the absence of grain boundaries. However, interfacial degradation remains a persistent concern. High-voltage operation (>4.5 V *vs.* Li/Li^+) accelerates side reactions between LRMs and SSEs, resulting in the formation of gaseous and solid byproducts, interphase thickening, and rapid capacity fading. The dissolution of TM, particularly Mn, into the SSE further destabilizes the interface and leads to parasitic reactions at the anode.

The interface between the cathode and the SSE represents a critical bottleneck in realizing stable high-performance ASSBs. SCLRM cathodes, when coupled with compatible SSEs, offer a promising avenue to mitigate such degradation pathways. However, the voltage window mismatch and chemical reactivity at the interface limit the realization of full LRM capacity.[90] For example, sulfide-based SSEs possess high ionic conductivity and mechanical softness, yet suffer from oxidative instability above 4.5 V, particularly when paired with oxygen-redox-active materials like LRMs. Localized decomposition of sulfide SSEs under uneven voltage distribution can form interfacial voids, degrade contact, and impede Li^+ transport. In Fig. 9b, cycling-induced morphological changes at the interface between the polymer electrolyte and the Li metal anode illustrate how initially tight interfacial contact deteriorates over time, disrupting Li^+ deposition behavior and increasing cell impedance.[87] Moreover, oxygen evolution and associated irreversible redox reactions in LRMs not only reduce coulombic efficiency but also lead to internal stress and interface passivation. As shown in Fig. 9c, uneven oxygen redox and localized side reactions contribute to interfacial void formation and reduced Li^+ diffusion kinetics.[88] The solid-solid interface is also affected by space charge accumulation due to chemical potential differences between the SSE and the active material, particularly in sulfide systems. This leads to polarization and hinders the activation of the Li_2MnO_3 component within the LRM structure. In this context, oxide SSEs provide a wider electrochemical window and higher thermal stability, but are

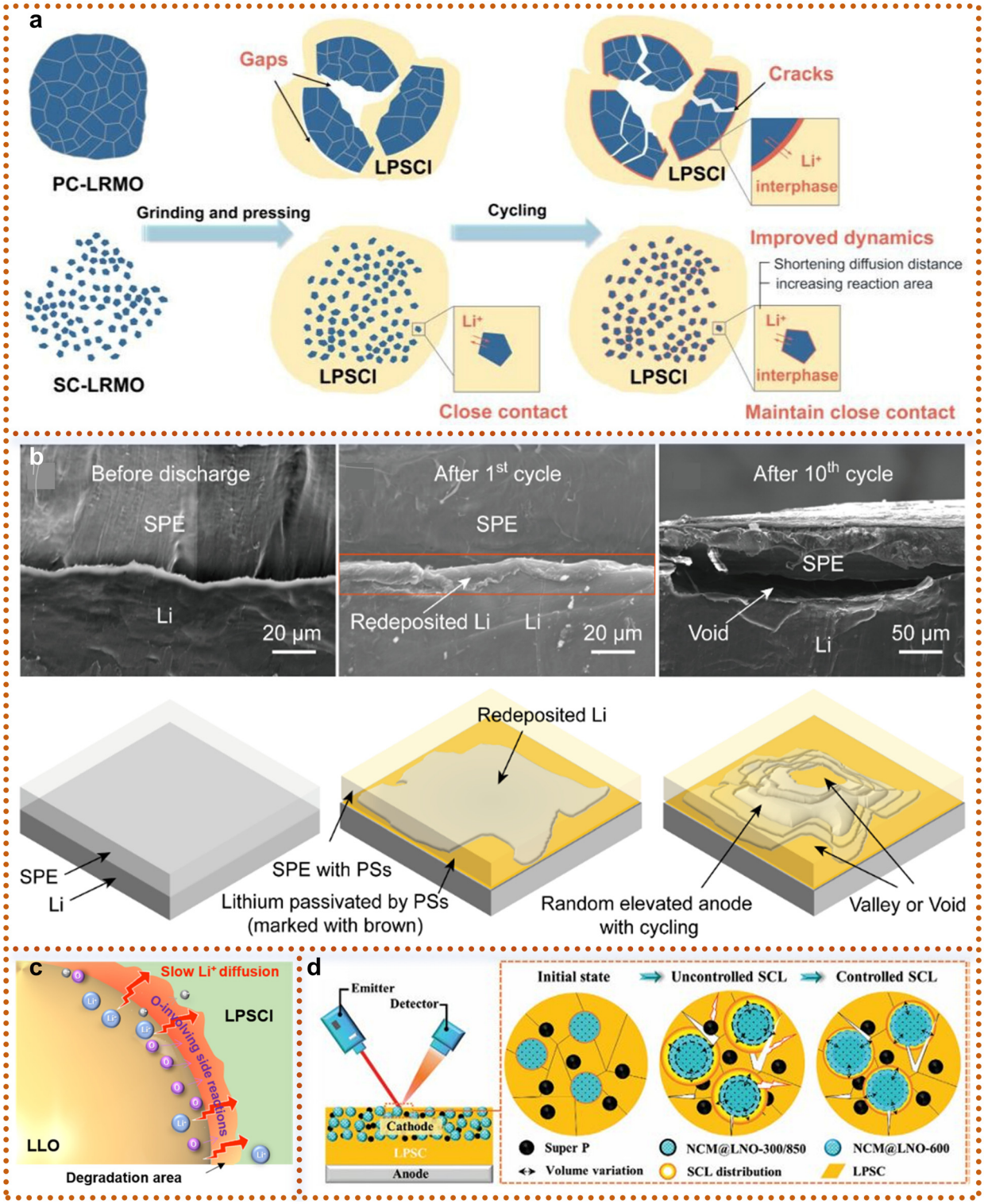

Fig. 9 Advances and challenges in applying SCLRMs to ASSBs. (a) Schematic illustration of the effect of micromorphology on mechanical pressure. Reproduced from ref. 82, copyright 2024 ACS. (b) Schematic diagram of SEM cross-section and failure mechanism in the cycling process. Reproduced from ref. 87, copyright 2021 Wiley-VCH. (c) Schematic diagram of slow Li^+ diffusion. Reproduced from ref. 88, copyright 2023 Wiley-VCH. (d) SCL evolution mechanism. Reproduced from ref. 89, copyright 2024 Wiley-VCH.

limited by rigid interfaces and high sintering temperatures.[91] Halide SSEs offer an attractive balance between ionic conductivity, chemical stability, and ease of processing.[92] Polymer SSEs, while inferior in conductivity, deliver superior mechanical flexibility and compatibility with SCLRMs.[93] Despite these advances, the degradation mechanisms at the cathode/SSE interface remain insufficiently understood. As illustrated in Fig. 9d, the formation of space charge layers and Li^+ depletion zones further hinders ionic transport across the interface.[89] Going forward, research must prioritize the development of composite cathode architectures integrating SCLRMs with SSEs *via* co-sintering or infiltration, as well as interfacial engineering approaches that stabilize redox reactions, suppress stress accumulation, and buffer chemical mismatches. In conclusion, SCLRMs hold substantial promise for ASSBs due to their mechanical robustness and microstructural uniformity, but achieving durable performance requires simultaneous innovation in particle design, electrolyte chemistry, and interfacial stabilization strategies.

Similar interface issues also exist on the lithium metal anode side in ASSBs: (i) unlike liquid electrolytes that can penetrate electrodes freely, solid electrolytes have a limited contact area with electrodes, hindering ion transport. This rigid contact generates structural stress during cycling, leading to increased interface impedance. (ii) Most solid electrolytes are chemically unstable against lithium metal, causing side reactions that further raise interface resistance. (iii) The rigid interface cannot accommodate the large volume changes of lithium metal during cycling, creating stress that mechanically damages the interface. (iv) The lithium deposition–dissolution process is not fully reversible.[94–96] Uneven ion channels promote the growth of mossy lithium structures, whose fracture creates "dead" lithium.[97] These issues can be mitigated by applying external stack pressure, filling interface gaps, and modifying the anode interface. Achieving compatibility between SCLRMs, solid-state electrolytes, and Li metal anodes is a research focus in solid-state batteries.

6. Research hotspots and new paradigms

Given that the research on SCLRMs is still in its early stages, most of the current understanding of degradation mechanisms stems from conventional LRMs, which have been the primary focus of studies over the past decade.[98] These conventional systems, developed earlier and tested under a variety of conditions, have laid the foundation for *in situ* techniques that enable dynamic tracking of structural, interfacial, and electrochemical evolution.[99] *In situ* transmission electron microscopy (TEM) has been widely applied in conventional LRMs to visualize oxygen release, TM migration, and microcrack propagation (Fig. 10a).[100] When transferred to SCLRMs, it could help assess whether such degradation features occur uniformly or manifest as localized distortions within large, defect-minimized grains.[101] Similarly, synchrotron radiation X-ray diffraction (SR-XRD), extensively used to monitor phase transitions from layered to spinel or rock-salt phases in conventional materials, can now be leveraged to determine whether SC integrity suppresses such transitions or delays their onset.[102] In addition, cryogenic electron microscopy (cryo-EM) and electron energy loss spectroscopy (EELS), which have revealed native interfacial compositions and oxygen-related redox activity in conventional LRMs (Fig. 10b), may offer insights into whether the smoother surfaces of SCLRMs promote more uniform CEI formation.[103] DEMS used to track O_2 and CO_2 evolution during high-voltage charging in conventional systems can help evaluate whether gas release kinetics differ in SC materials (Fig. 10c).[104] Notably, electrochemical impedance spectroscopy (EIS) has shown that conventional LRMs typically experience a rise in interfacial resistance at around 4.4 V, corresponding to Li_2MnO_3 activation (Fig. 10d).[105] In SCLRMs, EIS could clarify whether such impedance shifts are attenuated due to more coherent morphology. Likewise, *in situ* Raman spectroscopy has detected peroxo-type O–O vibrational modes in conventional materials (Fig. 10e), suggesting oxygen redox participation.[106] While signals in dense SCLRMs may be less intense, future application of Raman mapping under optimized conditions could yield valuable redox information. Together, these *in situ* techniques provide a methodological basis for uncovering the real-time degradation behavior of SCLRMs. Their adaptation will be key to evaluating whether SC architectures truly alleviate typical structural and interfacial failure modes.

While *in situ* structural diagnostics have clarified how lattice strain, phase transitions, and interfacial layers evolve under electrochemical cycling, they do not fully explain the origins of capacity fading or voltage hysteresis in lithium-rich cathodes. To address these phenomena, it is essential to investigate the underlying redox mechanisms, particularly the coupled cationic (TM) and anionic (lattice oxygen) redox processes that govern charge compensation and energy delivery. Although SCLRMs exhibit more ordered structures and reduced surface reactivity, the diagnostic strategies developed for conventional materials remain directly applicable and offer critical insights into their redox behavior. Extended X-ray absorption fine structure (EXAFS) has been widely employed to probe local TM coordination and oxidation states in conventional LRMs. Feng Wu *et al.* reported that antisite defects formed under high-voltage conditions contribute to structural stabilization by accommodating internal stress and delaying phase transition onset (Fig. 10f).[107] Whether such defect-mediated stabilization pathways exist or are suppressed in SCLRMs remains an open question that EXAFS can help resolve. In parallel, multiscale imaging by Jun Lu *et al.* revealed that heterogeneous oxygen redox activity in conventional particles leads to the formation of nanopores, TM dissolution, and localized structural collapse (Fig. 10g).[108] Applying similar approaches to SCLRMs could determine whether the coherent lattice mitigates such spatially confined degradation.[114] Further insights into oxygen redox have been gained using resonant inelastic X-ray scattering (RIXS) and soft transmission

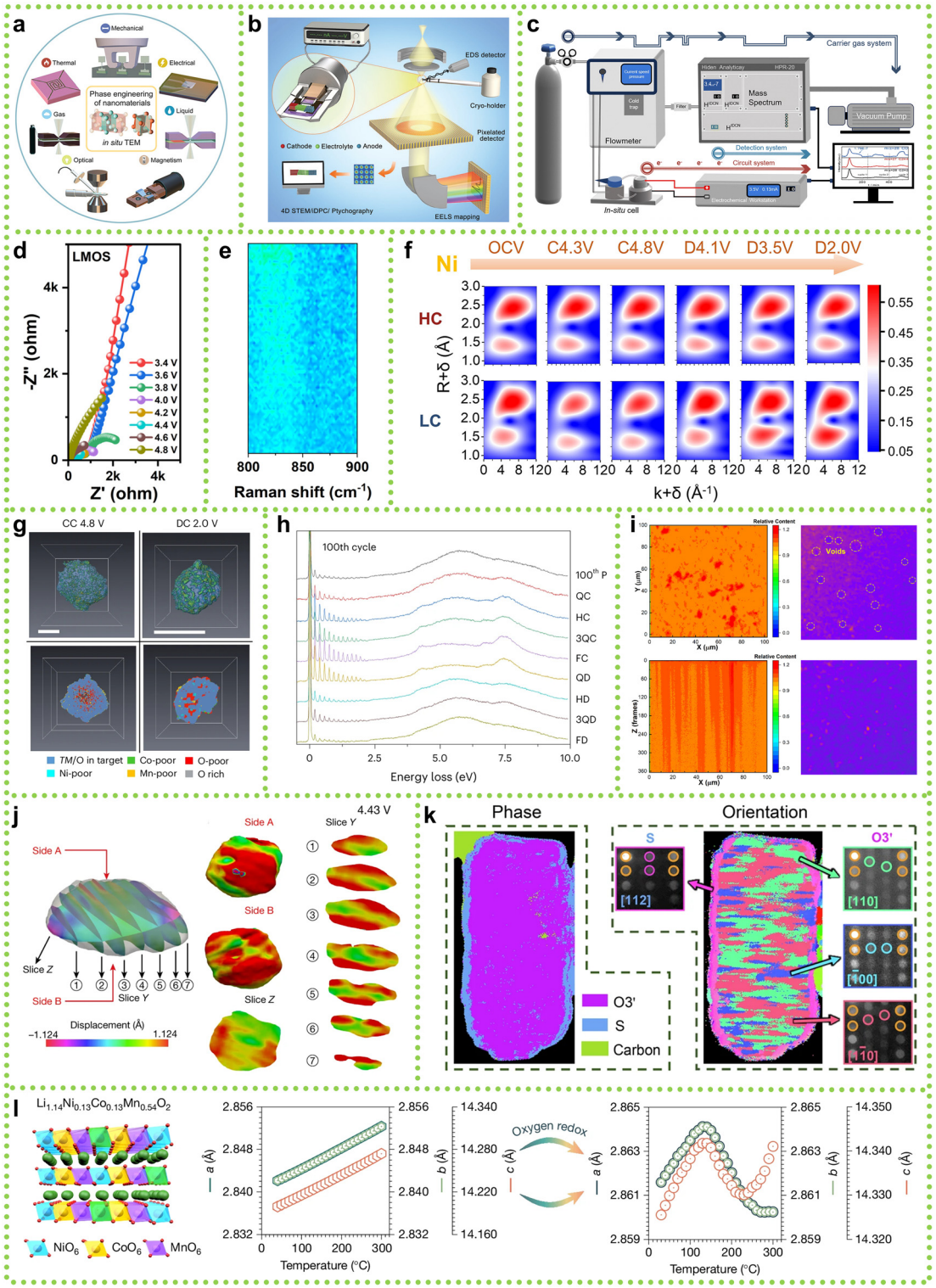

Fig. 10 Prospective advanced analytical methods for understanding the energy storage mechanisms of SCLRMs. (a) *In situ* TEM. Reproduced from ref. 100, copyright 2023 ACS. (b) Cryo-TEM. Reproduced from ref. 103, copyright 2021 Elsevier. (c) DEMS. Reproduced from ref. 104, copyright 2025 RSC. (d) *In situ* EIS. Reproduced from ref. 105, copyright 2024 Elsevier. (e) *In situ* Raman spectra. Reproduced from ref. 106, copyright 2025 Elsevier. (f) EXAFS spectra with k^3-weighted. Reproduced from ref. 107, copyright 2025 Elsevier. (g) Soft TXM. Reproduced from ref. 108, copyright 2024 NPG. (h) RIXS spectra. Reproduced from ref. 109, copyright 2024 NPG. (i) TOF-SIMS. Reproduced from ref. 110, copyright 2025 Elsevier. (j) *In situ* BCDI. Reproduced from ref. 111, copyright 2022 NPG. (k) 4D-STEM. Reproduced from ref. 112, copyright 2025 NPG. (l) Negative thermal expansion. Reproduced from ref. 113, copyright 2025 NPG.

X-ray microscopy (TXM). Peter G. Bruce *et al.* employed RIXS to detect trapped molecular O_2 within conventional LRMs, showing that oxygen redox irreversibility increases with cycling (Fig. 10h).[109] These methods could help elucidate whether oxygen retention and reversibility are improved in SCLRMs due to suppressed stress gradients. Complementary studies using nuclear magnetic resonance (NMR) spectroscopy have correlated the formation of Li–O_2 domains and pore expansion with voltage decay. Whether similar degradation pathways occur in SC frameworks, where porosity is minimal, remains to be verified. In addition, Qiang Zhang *et al.* combined time-of-flight secondary ion mass spectroscopy (TOF-SIMS) with X-ray computed tomography (XCT) to visualize lithium distribution and void formation at the cathode–electrolyte interface during charging (Fig. 10i).[110] In conventional systems, oxygen evolution was found to disrupt lithium transport pathways and degrade interface contact. Applying this approach to SCLRMs could determine whether surface densification and structural integrity reduce such adverse effects and promote stable lithium utilization.[115]

Following redox mechanism analysis, understanding how such processes translate into long-term structural degradation and interfacial failure is critical for evaluating the practical viability of lithium-rich cathodes. In conventional LRM materials, stress accumulation, grain boundary fracture, and unstable electrode–electrolyte interfaces have been extensively reported as major contributors to capacity fading. These degradation modes, although specific to polygranular and defect-rich systems, offer a valuable framework for interpreting how similar or distinct failure mechanisms may evolve in SCLRMs. Bragg coherent diffraction imaging (BCDI) has been successfully applied to visualize three-dimensional strain evolution in conventional LRMs. Feng Pan *et al.* observed that delithiation-induced tensile strain originated near particle surfaces and progressively expanded inward, triggering oxygen release and structural collapse (Fig. 10j).[111] The use of BCDI in SCLRMs could reveal whether the absence of grain boundaries suppresses such strain gradients or simply redistributes them across different crystallographic directions. Similarly, *in situ* neutron diffraction and four-dimensional scanning transmission electron microscopy (4D-STEM), as employed by Yinguo Xiao *et al.*, uncovered core–shell structural transformations, interlayer stress, and defect coalescence during extended cycling (Fig. 10k).[112] These techniques can be used to determine whether the more continuous lattice in SCLRMs inhibits such intralayer defect formation or merely delays its onset. Thermal stability is another important dimension of structural robustness. Zhaoping Liu *et al.* identified anomalous negative thermal expansion in conventional LRMs and established a quantitative link between oxygen redox activity and lattice contraction, offering a predictive descriptor for thermomechanical reliability.[113] Applying such dynamic structural disorder analysis to SCLRMs may determine whether reduced oxygen volatility improves thermal tolerance or introduces new expansion–contraction mismatches at high states of charge. Collectively, these structural and interfacial probing techniques have provided critical insights into the interplay between redox activity and mechanical stress in conventional lithium-rich systems. Their application in SCLRMs is essential to assess whether single-crystal morphology offers practical gains in structural and interfacial stability.

7. Vision for next-generation systems

As research on LRMs progresses toward next-generation applications, SC variants have emerged as promising candidates due to their intrinsic structural uniformity and enhanced thermal-mechanical robustness. However, these advantages also introduce unique scientific challenges. Unlike conventional PCLRM materials, SCLRMs possess coherent crystalline lattices with minimal internal defects, reducing the number of observable degradation features. This structural integrity, while beneficial for stability, complicates the early detection of performance deterioration using standard diagnostic techniques. Although *in situ* and operando methods such as Raman spectroscopy, synchrotron-based diffraction, and transmission electron microscopy have proven effective in PC systems, their spatial resolution and sensitivity remain insufficient for capturing subtle transformations in SC materials. The high cost also restricts the large-scale application of high-throughput characterization. Consequently, there is a growing emphasis on integrating AI into material characterization and optimization (Fig. 11). Piyasan Praserthdam *et al.* introduced high-throughput phase prediction of high-entropy alloys using an algorithm combining the Korringa–Kohn–Rostoker coherent potential approximation (KKR-CPA) with artificial neural networks (ANN).[116] AI-enhanced modeling approaches, informed by density functional theory and large-scale data sets, enable the prediction of critical descriptors including lattice strain tolerance, oxygen vacancy formation energy, and migration tendencies of TM ions.[117] These parameters are directly linked to voltage fading, oxygen instability, and irreversible phase transformations. AI can also support interface engineering by simulating cathode–electrolyte interactions and predicting Li^+ diffusion barriers, reaction enthalpies, and interfacial phase equilibria. This facilitates the rational design of surface coatings and interlayers that stabilize the interface while preserving redox activity.[118] Wen bin Hu and his team utilized an AI-driven K-means clustering algorithm to accurately identify the optimal "golden combination" from hundreds of candidates, successfully developing a 600 Wh kg^{-1}-level "AI electrolyte".[119] Additionally, graph-based deep learning models trained on structural and electronic databases can accelerate the discovery of dopants and surface terminations that mitigate side reactions and stabilize anionic redox chemistry. As the path from laboratory synthesis to practical implementation remains complex, the predictive capability of AI offers a systematic approach to optimize SCLRMs under the design constraints of next-generation solid-state batteries.[120] Inchul Park *et al.* developed an unsupervised analytical framework that leverages Principal Component Analysis (PCA) on a

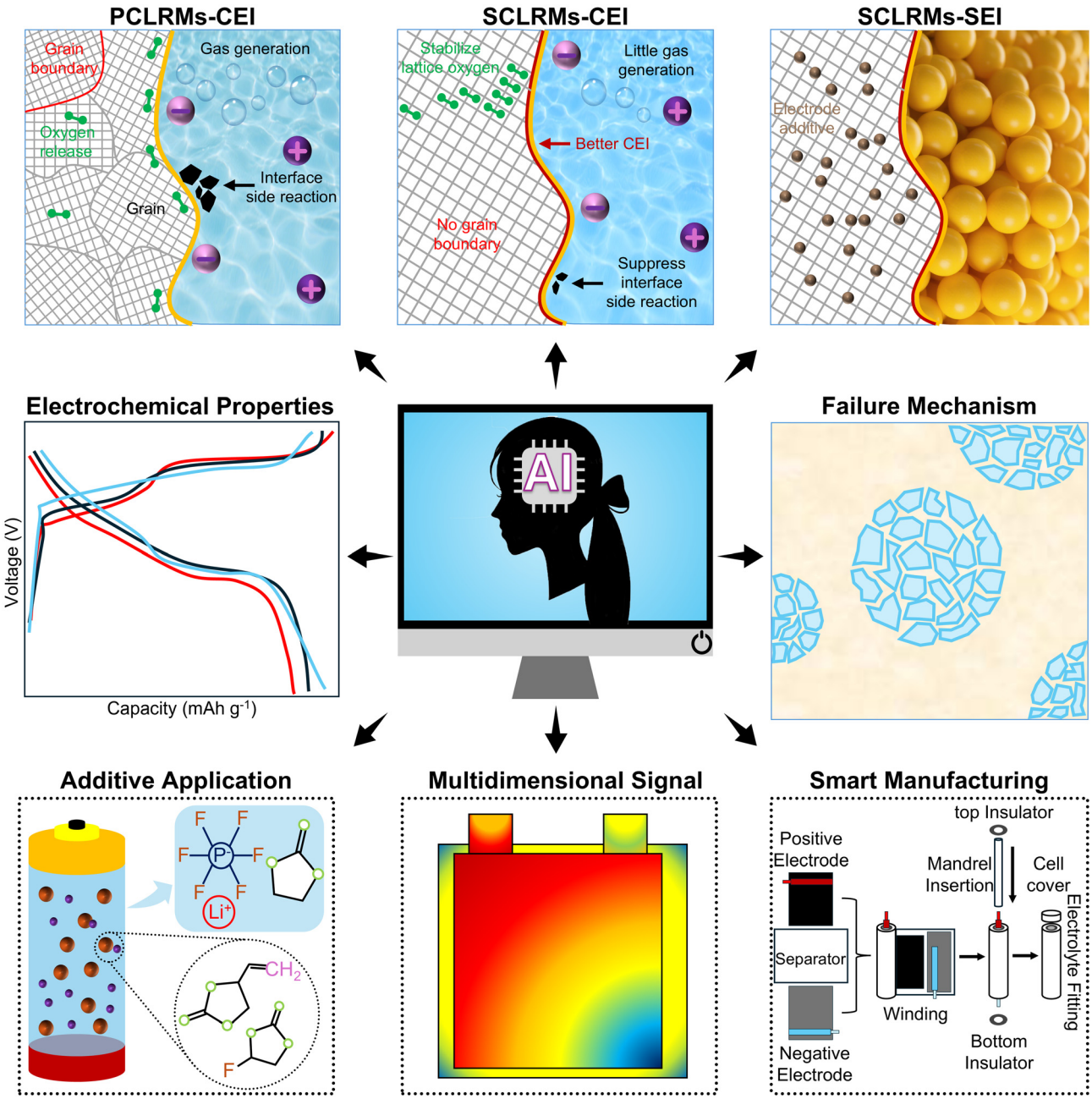

Fig. 11 AI applied in battery includes electrolyte interface analysis, properties upgrading, failure mechanism calculation, additive screening, multidimensional signal acquisition, and intelligent manufacturing.

large dataset of over 30 000 LRM charge curves to identify fundamental degradation factors and enhance predictability.[121] These developments signify a paradigm shift from empirical trial-and-error strategies to data-driven design, ultimately unlocking more efficient and reliable pathways for SCLRMs in commercial energy storage.

While the discovery of AI-assisted materials provides a foundation for developing high-performance SC cathodes, realizing their full potential requires continuous performance monitoring and intelligent response mechanisms during real-world operation. The structural integrity of SCLRMs minimizes common degradation issues such as particle pulverization and intergranular cracking. However, it also conceals subtle indicators of early failure, including lattice microstrain, localized oxygen loss, and interfacial fatigue. These phenomena are often undetectable by conventional battery management systems that rely on macroscopic voltage, current, and temperature data. To address this, the integration of embedded sensor systems into battery architectures is becoming increasingly important.[122] Recent studies have demonstrated the feasibility of incorporating microscale sensors capable of monitoring thermal gradients, mechanical stress, and electro-

chemical shifts *in situ*. When combined with machine learning algorithms capable of processing complex, time-resolved datasets, these sensors enable real-time state estimation and fault prediction.[123] For example, thin-film sensors resistant to electrochemical corrosion can be implanted within SCLRM-based cells without compromising structural or electrochemical integrity. Communication modules employing carrier-wave technology allow signal transmission through metal casings, overcoming electromagnetic shielding issues. Such systems, once trained on extensive cycling data, can detect deviation patterns and anticipate failure before catastrophic events occur. Battery intelligence is evolving through three functional stages. First-generation systems offer real-time sensing and data acquisition. Second-generation platforms integrate dynamic response capabilities such as self-regulation, self-protection, and thermal balancing. Looking ahead, third-generation smart batteries will be equipped with predictive control algorithms and cloud-connected infrastructure, enabling autonomous decision-making in response to both external conditions and internal degradation signatures.[124–126] For high-capacity materials like SCLRMs, this level of system intelligence will be crucial to manage their complexity and ensure both safety and performance across extended lifetimes.

Looking to the future, the integration of SCLRMs into high-performance energy storage systems will depend on coordinated advances across synthesis, interface design, system intelligence, and manufacturing scalability. The evolution from PCLRMs to SCLRMs and further into ASSB platforms involves addressing several technological bottlenecks.[127,128] These include the complexity of current high-temperature synthesis routes, challenges in electrolyte compatibility, interfacial mismatch under cycling conditions, and mechanical instability induced by anisotropic volume changes. Addressing these challenges requires a unified approach across multiple scales. On the materials front, developing one-step, low-temperature synthesis protocols with precise control over crystal growth and particle morphology will be essential for industrial viability. At the interfacial level, new coating strategies, compositional gradients, and engineered interphases must be employed to alleviate mechanical mismatch and stabilize lithium transport. From a systems perspective, embedding intelligent diagnostic and control frameworks within the battery platform will be essential to ensure safety and longevity.[129] AI offers significant value here by enabling high-throughput screening of candidate materials, real-time condition monitoring, and optimization of battery operation under variable load conditions. Furthermore, intelligent manufacturing approaches can be applied to enhance yield control, quality assurance, and process reproducibility.[130] As battery applications expand into more demanding domains such as electric aviation, smart mobility, and grid-level storage, the importance of integrating high-capacity, structurally stable, and self-adaptive materials will only grow.[131–133] SCLRMs, with their high theoretical capacity and interface adaptability, offer a viable route to meet these demands. Their successful application will depend on the convergence of predictive materials design, adaptive system intelligence, and scalable manufacturing technologies.[134,135] The future of energy storage lies not only in advanced materials but also in the systems that can intelligently harness and manage their potential in dynamic and real-world environments.

8. Conclusion and outlook

This review has systematically summarized the recent advances, challenges, and opportunities related to SCLRMs, particularly in their transition from conventional layered cathodes toward application in ASSB systems and the irreversible shift toward intelligent battery technologies in the coming years. The abundance and low cost of manganese make LRMs environmentally and economically attractive for large-scale deployment compared with other cathodes. Furthermore, compared with PCLRMs, SCLRMs possess more ordered lattices, reduced grain boundaries, and higher compacted density, contributing to improved structural integrity and cycling stability. These advantages suppress particle pulverization and intergranular cracking during delithiation/relithiation, while also enabling better compatibility with the high-pressure environments required in ASSBs. By integrating solid-state electrolytes with SCLRMs, battery safety and energy density can be simultaneously enhanced. SCLRM-based ASSBs are projected to achieve energy densities exceeding 1000 Wh kg^{-1} while minimizing thermal runaway risk, offering strong potential for future electric mobility and grid storage. Importantly, this review highlights the growing role of *in situ* and operando characterization techniques in elucidating the structural and interfacial behaviors of SCLRMs under realistic working conditions. These tools have proven indispensable in visualizing phase transitions, tracking oxygen redox reversibility, and evaluating degradation pathways across length scales. The evolution from PCLRMs to SCLRMs and ultimately to practical ASSB integration involves key bottlenecks including synthesis complexity, interfacial instability, and structural mismatches. Overcoming these barriers requires coordinated efforts in materials chemistry, crystal engineering, and system-level integration. The findings and perspectives presented herein provide a scientific foundation for guiding future research and technological translation of SCLRMs into high-performance solid-state energy storage systems.

Looking ahead, the practical implementation of SCLRMs in solid-state batteries will depend on resolving several material, interfacial, and manufacturing challenges. Although SCLRMs exhibit superior crystallinity and mechanical robustness, their current synthesis routes often involve energy-intensive, multi-step thermal treatments. Future efforts must aim to simplify production through one-step calcination, reduce sintering temperatures, and achieve uniform particle sizes to balance cost, crystallinity, and electrochemical performance. In parallel, mechanistic studies on size-dependent redox behavior, ion transport, and degradation pathways specific to SC morphologies will be crucial for refining design principles. In addition to synthesis, interface instability remains a key limit-

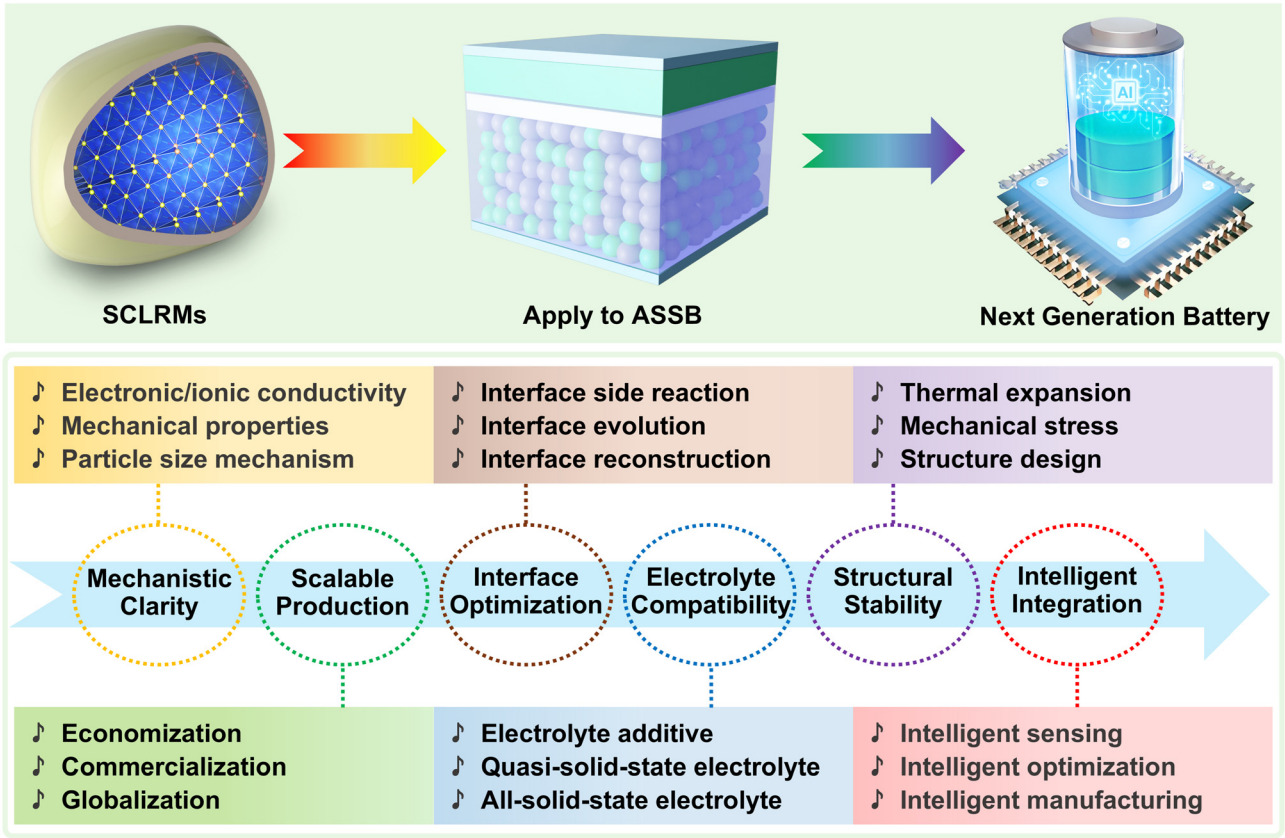

Fig. 12 Visionary development blueprint of SCLRMs.

ation for SCLRM-based ASSBs. Mechanical stress, poor ionic contact, and chemical incompatibility at the electrode–electrolyte interface can lead to rapid performance loss. The development of tailored interfacial layers and the selection of thermodynamically stable solid-state electrolytes are critical to mitigate these issues. Furthermore, real-time *in situ* techniques must be continuously advanced to provide spatially resolved insight into interfacial reactions and redox dynamics, thereby informing material selection and structural design. The participation of lattice oxygen anions in redox reactions for charge compensation provides a critical pathway to surpass the capacity limit of traditional TM cations. However, this process is accompanied by irreversible oxygen release, detrimental surface phase reconstruction, and the continuous accumulation of oxygen vacancies. These issues lead to severe voltage decay, capacity loss, and gassing side reactions, constituting a cardinal bottleneck for their commercial viability. Therefore, the current research priority is to systematically leverage and advance advanced *in situ* characterization techniques—such as synchrotron-based X-ray absorption spectroscopy, *in situ* differential electrochemical mass spectrometry, and *in situ* Raman spectroscopy. These tools enable the real-time monitoring of dynamic lattice oxygen evolution, transient intermediate species, and interfacial side reactions during actual battery operation. Through precise interpretation of this dynamic information, we can establish a structure–activity relationship linking "microscopic atomic structure" to "macroscopic electrochemical performance". This provides crucial theoretical guidance and experimental basis for the targeted optimization of materials (*e.g.*, *via* surface coating or lattice doping) to stabilize the oxygen lattice framework and enhance its reaction reversibility. In particular, AI technologies offer powerful tools to accelerate the development of SCLRMs-ASSBs. Machine learning models can rapidly screen cathode–electrolyte combinations, predict structural stability, and guide synthesis parameter optimization. Moreover, AI-integrated smart battery systems can enable self-monitoring and adaptive control during operation, improving safety and lifespan. As outlined in Fig. 12, the transition from SCLRMs to ASSBs and finally to smart battery architectures defines a forward-looking roadmap. Realizing the full potential of SCLRMs will require cross-disciplinary innovation in materials design, advanced characterization, and intelligent system integration, paving the way toward safer, higher-performing, and commercially viable next-generation energy storage technologies.

Author contributions

The manuscript was written through the contributions of all authors. All authors have approved the final version of the manuscript.

Conflicts of interest

The authors declare no competing financial interest.

Data availability

No primary research results, software or code have been included and no new data were generated or analysed as part of this review.

Acknowledgements

This work was supported by the National Natural Science Foundation of China (22179008) and the Yibin 'Jie Bang Gua Shuai' (2022JB004). L. Chen acknowledges the support from the High-Level Talent Introduction Project of Yibin (2024YG03). J. Y. Dong acknowledges the support from the Postdoctoral Fellowship Program of CPSF (GZB20230931) and the Special Support of Chongqing Postdoctoral Research Project (2023CQBSHTB2041).

References

1 Y. X. Yao, L. Xu, C. Yan and Q. Zhang, *EES Batteries*, 2025, **1**, 9–22.
2 W. Yang, W. Chen, H. Zou, J. Lai, X. Zeng, Y. Zhang, X. Zeng, K. Ding, S. Zhang, L. Ma, Z. Li and Q. Zheng, *Angew. Chem., Int. Ed.*, 2025, **64**, e202424353.
3 Z. Sun, F. Li, J. Ding, Z. Lin, M. Xu, M. Zhu and J. Liu, *ACS Energy Lett*, 2023, **8**, 2478–2487.
4 A. Manthiram, *Nat. Commun.*, 2020, **11**, 1550.
5 J. Xiao, X. Cao, B. Gridley, W. Golden, Y. Ji, S. Johnson, D. Lu, F. Lin, J. Liu, Y. Liu, Z. Liu, H. N. Ramesh, F. Shi, J. Schrooten, M. J. Sims, S. Sun, Y. Shao, A. Vaisman, J. Yang and M. S. Whittingham, *Chem. Rev.*, 2025, **125**, 6397–6431.
6 P. Xu, Y. C. Gao, Y. X. Huang, Z. Y. Shuang, W. J. Kong, X. Y. Huang, W. Z. Huang, N. Yao, X. Chen, H. Yuan, C. Z. Zhao, J. Q. Huang and Q. Zhang, *Adv. Mater.*, 2024, **36**, 2409489.
7 N. Y. Park, H. U. Lee, T. Y. Yu, I. S. Lee, H. Kim, S. M. Park, H. G. Jung, Y. C. Jung and Y. K. Sun, *Nat. Energy*, 2025, **10**, 479–489.
8 Y. Gao, X. Ma, Y. Yan, S. Zhang, J. Liang, B. Li, F. Kang and D. Zhai, *Adv. Energy Mater.*, 2025, **15**, 2404913.
9 J. He, Y. Deng, J. Han, T. Xu, J. Qi, J. Li, Y. Zhang, Z. Zhao, Q. Li, J. Xiao, J. Zhang, D. Kong, W. Wei, S. Wu and Q. H. Yang, *Nat. Commun.*, 2025, **16**, 4858.
10 L. Peng, D. L. Mauzerall, Y. D. Zhong and G. He, *Nat. Commun.*, 2023, **14**, 4858.
11 Battery500: Progress Update, https://www.energy.gov/eere/articles/battery500-progress-update, (accessed 05–19, 2022).
12 J. Amici, P. Asinari, E. Ayerbe, P. Barboux, P. BayleGuillemaud, R. J. Behm, M. Berecibar, E. Berg, A. Bhowmik, S. Bodoardo, I. E. Castelli, I. CekicLaskovic, R. Christensen, S. Clark, R. Diehm, R. Dominko, M. Fichtner, A. A. Franco, A. Grimaud, N. Guillet, M. Hahlin, S. Hartmann, V. Heiries, K. Hermansson, A. Heuer, S. Jana, L. Jabbour, J. Kallo, A. Latz, H. Lorrmann, O. M. Lovvik, S. Lyonnard, M. Meeus, E. Paillard, S. Perraud, T. Placke, C. Punckt, O. Raccurt, J. Ruhland, E. Sheridan, H. Stein, J. M. Tarascon, V. Trapp, T. Vegge, M. Weil, W. Wenzel, M. Winter, A. Wolf and K. Edstrom, *Adv. Energy Mater.*, 2022, **12**, 2102785.
13 RISING2 FY2016~FY2020, https://www.rising.saci.kyoto-u.ac.jp/rising2/en/overview/, (accessed 02–27, 2020).
14 G. Wang, M. Xu, L. Fei and C. Wu, *Small*, 2024, **20**, e2405659.
15 B. Li, Z. Zhuo, L. Zhang, A. Iadecola, X. Gao, J. Guo, W. Yang, A. V. Morozov, A. M. Abakumov and J. M. Tarascon, *Nat. Mater.*, 2023, **22**, 1370–1379.
16 M. Zheng, X. Zhu, H. Zheng, Z. Bo and J. Lu, *Nat. Energy*, 2025, **10**, 789–792.
17 B. Li, K. Zhang, Y. Yang, Y. Zuo, X. Li and D. Xia, *Adv. Mater.*, 2024, **36**, 2400259.
18 S. Y. Luchkin, M. A. Kirsanova, D. A. Aksyonov, S. A. Lipovskikh, V. A. Nikitina, A. M. Abakumov and K. J. Stevenson, *ACS Appl. Energy Mater.*, 2022, **5**, 7758–7769.
19 Z. Zhang, Y. Li, X. Shen, L. Yang, C. Zhang, Y. Liu, B. Wang, C. Y. Kuo, S. C. Haw, C. T. Chen, C. w. Pao, H. Y. Huang, D. J. Huang, J. Ju, J. Ma, Z. Hu, Y. Gao, X. Wang, R. Yu, Z. Wang and L. Chen, *Adv. Mater.*, 2025, **37**, 2505724.
20 Y. Fang, Y. Su, J. Dong, J. Zhao, H. Wang, Y. Lu, B. Zhang, H. Yan, F. Wu and L. Chen, *J. Energy Chem.*, 2024, **92**, 250–262.
21 C. Zheng, Y. Wang, H. Mao, J. Zhang, X. Yang, J. Li, D. Zhang, X. Wang, F. Kang and J. Li, *Nat. Commun.*, 2025, **16**, 3900.
22 T. Wang, W. Zeng, J. Zhu, W. Tian, J. Wang, J. Tian, D. Yuan, S. Zhang and S. Mu, *Nano Energy*, 2023, **113**, 108577.
23 J. Guo, Y. Lai, X. Gao, S. Li, H. Zhang, C. Guan, L. Chen, Z. Yang, S. Li and Z. Zhang, *Energy Storage Mater.*, 2024, **69**, 103383.
24 H. Pan, S. Jiao, Z. Xue, J. Zhang, X. Xu, L. Gan, Q. Li, Y. Liu, X. Yu, H. Li, L. Chen and X. Huang, *Adv. Energy Mater.*, 2023, **13**, 2203989.
25 Y. Feng, L. Zhou, H. Ma, Z. Wu, Q. Zhao, H. Li, K. Zhang and J. Chen, *Energy Environ. Sci.*, 2022, **15**, 1711–1759.
26 X. He, J. Wang, L. Wang and J. Li, *Materials*, 2016, **9**, 661.
27 S. Kuppan, A. K. Shukla, D. Membreno, D. Nordlund and G. Chen, *Adv. Energy Mater.*, 2017, **7**, 1602010.
28 Z. Wu, C. Zhang, M. Zheng, C. Zeng, W. Yang and R. Shao, *EES Batteries*, 2025, **1**, 73–99.
29 X. Zhao, X. Cao, C. Sheng, L. Xu, P. Wu, Y. Zhou, P. He, Y. Tang and H. Zhou, *ACS Appl. Mater. Interfaces*, 2024, **16**, 24147–24161.

30 H. Li, H. Zhang, Y. Liang, R. Chen and Y. Cao, *Batteries Supercaps*, 2024, **8**, e202400443.
31 Z. Qin, Y. Zhang, W. Luo, T. Zhang, T. Wang, L. Ni, H. Wang, N. Zhang, X. Liu, J. Zhou and G. Chen, *Angew. Chem., Int. Ed.*, 2023, **62**, e202218672.
32 X. Yin, D. Li, L. Hao, Y. Wang, Y. Wang, X. Guo, S. Zhao, B. Wang, L. Wu and H. Yu, *Chem. Commun.*, 2023, **59**, 639–642.
33 Z. Fu, P. Yang, X. Luo, R. Li, Y. Shen, L. Liao, P. Luo, X. Li, B. Yu, M. Wang, J. Chen, Z. Ma, B. Guo, Y. Huang, S. Wang and X. Li, *Mater. Lett.*, 2024, **370**, 136820.
34 C. Jiao, M. Wang, B. Huang, M. Zhang, G. Xu, Y. Liu, Y. Zhao and X. Hu, *J. Alloys Compd.*, 2023, **937**, 168389.
35 M. M. Yuan, L. D. Wang, J. Zhang, M. J. Ran, K. Wang, Z. Y. Hu, G. Van Tendeloo, Y. Li and B. L. Su, *J. Colloid Interface Sci.*, 2024, **674**, 238–248.
36 M. H. Rossouw and M. M. Thackeray, *Mater. Res. Bull.*, 1991, **26**, 463–473.
37 K. Numata, C. Sakaki and S. Yamanaka, *Chem. Lett.*, 1997, **26**, 725–726.
38 K. Numata, C. Sakaki and S. Yamanaka, *Solid State Ionics*, 1999, **117**, 257–263.
39 Z. H. Lu, Z. H. Chen and J. R. Dahn, *Chem. Mater.*, 2003, **15**, 3214–3220.
40 S. Xu, Z. Chen, W. Zhao, W. Ren, C. Hou, J. Liu, W. Wang, C. Yin, X. Tan, X. Lou, X. Yao, Z. Gao, H. Liu, L. Wang, Z. Yin, B. Qiu, B. Hu, T. Li, C. Dong, F. Pan and M. Zhang, *Energy Environ. Sci.*, 2024, **17**, 3807–3818.
41 A. R. Armstrong, M. Holzapfel, P. Novak, C. S. Johnson, S. H. Kang, M. M. Thackeray and P. G. Bruce, *J. Am. Chem. Soc.*, 2006, **128**, 8694–8698.
42 Z. Zhu, D. Yu, Y. Yang, C. Su, Y. Huang, Y. Dong, I. Waluyo, B. Wang, A. Hunt, X. Yao, J. Lee, W. Xue and J. Li, *Nat. Energy*, 2019, **4**, 1049–1058.
43 J. Sun, C. Sheng, X. Cao, P. Wang, P. He, H. Yang, Z. Chang, X. Yue and H. Zhou, *Adv. Funct. Mater.*, 2021, **32**, 2110295.
44 S. Sun, C. Z. Zhao, H. Yuan, Z. H. Fu, X. Chen, Y. Lu, Y. F. Li, J. K. Hu, J. Dong, J. Q. Huang, M. Ouyang and Q. Zhang, *Sci. Adv.*, 2022, **8**, eadd5189.
45 T. Zhao, R. Ji and Y. Meng, *Chem. Phys. Lett.*, 2019, **730**, 354–360.
46 X. Cui, J. Zhou, H. Ding, X. Cai, J. Zhang, X. Hu, J. Zhang, X. Li, J. Zhu, N. Zhang and S. Li, *J. Power Sources*, 2024, **623**, 235458.
47 Z. Ren, G. Li, X. Bai, W. Hu, X. Li, H. He, Z. Chang, Y. Liu, Z. Wang, Z. Liang, L. Guo, Z. Gao and J. Wang, *Electrochim. Acta*, 2023, **461**, 142630.
48 J. Li, H. Lin, C. Tang, D. Yu, J. Sun, W. Zhang and Y. Wang, *Nanotechnology*, 2021, **33**, 065705.
49 J. Sun, X. Cao, W. Yang, E. Yoo and H. Zhou, *J. Mater. Chem. A*, 2023, **11**, 13956–13964.
50 L. T. Li, Y. F. Chen, Y. C. Liu, Q. Zhang, J. W. Wu and Q. H. Yuan, *Rare Met.*, 2023, **42**, 830–837.
51 M. Yoon, Y. Dong, Y. Huang, B. Wang, J. Kim, J. S. Park, J. Hwang, J. Park, S. J. Kang, J. Cho and J. Li, *Nat. Energy*, 2023, **8**, 482–491.
52 H. Wu, J. Dong, Y. Zhang, L. Lin, G. Gao, T. Li, X. Yi, B. Sa, J. Wang, L. Wang, J. Li, K. Amine, D. L. Peng and Q. Xie, *Adv. Funct. Mater.*, 2023, **33**, 2303707.
53 J. Zhao, Y. Su, J. Dong, Q. Shi, Y. Lu, N. Li, H. Wang, Y. Fang, W. Li, J. Hao, Y. Wu, Q. Qi, F. Wu and L. Chen, *Energy Storage Mater.*, 2024, **70**, 103550.
54 Y. Yu, Q. Li, H. Peng, X. Zhou, Y. Wang, F. Liu, H. Wang, G. Wang, G. Van Tendeloo and J. Wu, *Small*, 2025, **21**, 2501899.
55 T. Wu, X. Zhang, Y. Wang, N. Zhang, H. Li, Y. Guan, D. Xiao, S. Liu and H. Yu, *Adv. Funct. Mater.*, 2023, **33**, 2210154.
56 B. Zhang, Y. Zhang, H. Wu, L. Zeng, X. Wang, H. Liu, X. Wu, J. Chen, H. Zhang, Y. Yan, Y. Tang, H. Huang, L. Zheng, Q. Zhang, Q. Xie, D. L. Peng, C. Li, Y. Qiao and S. G. Sun, *Energy Storage Mater.*, 2023, **62**, 102926.
57 L. Yan, Y. Gao, M. Chen, C. Zhao, S. Yang, C. Chen, J. Li, Y. Li, K. Wang, H. Wang, J. Li, H. Zhang and J. Mao, *ACS Appl. Mater. Interfaces*, 2024, **16**, 60166–60179.
58 X. Sun, C. Qin, B. Zhao, S. Jia, Z. Wang, T. Yang, X. Liu, L. Pan, L. Zheng, D. Luo and Y. Zhang, *Energy Storage Mater.*, 2024, **70**, 103559.
59 X. Gao, L. Wang, J. Guo, S. Li, H. Zhang, L. Chen, Y. Zhang, Y. Lai and Z. Zhang, *Adv. Funct. Mater.*, 2024, **34**, 2407692.
60 J. Hwang, S. Myeong, E. Lee, H. Jang, M. Yoon, H. Cha, J. Sung, M. G. Kim, D. H. Seo and J. Cho, *Adv. Mater.*, 2021, **33**, 2100352.
61 Z. Li, C. Guo, S. Cao, H. Li, J. Chen, L. Wu, R. Wang, Y. Bai and X. Wang, *J. Alloys Compd.*, 2024, **984**, 2201522.
62 J. Dong, F. Wu, J. Y. Zhao, Q. Shi, Y. Lu, N. Li, D. Cao, W. Li, J. Hao, X. Yang, L. Chen and Y. Su, *Energy Storage Mater.*, 2023, **60**, 102798.
63 C. Yang, J. Luo, J. Zhang, Y. Cheng, H. Wang, Y. Ge, Q. Tong, J. Tong, R. Liu, W. D. Liu, Y. Chen and Z. Yu, *Adv. Funct. Mater.*, 2026, **36**, e11737.
64 L. Wang, L. Xu, W. Xue, Q. Fang, H. Liu, Y. Liu, K. Zhou, Y. Li, X. Wang, X. Wang, X. Yang, X. Yu and X. Wang, *Nano Energy*, 2024, **121**, 109241.
65 Y. Li, Y. C. Yin, W. Shu, L. Xian, Q. Zhang, G. Chen, C. Zeng, W. Zeng, W. Ao and J. Yang, *Adv. Funct. Mater.*, 2025, **35**, 2419603.
66 W. Zeng, F. Liu, J. Yang, B. Zhang, F. Cao, W. Tian, J. Wang, R. Yu, F. Xia, H. Peng, J. Ma, Z. Wang, S. Mu and J. Wu, *Energy Storage Mater.*, 2023, **54**, 651–660.
67 Y. Yang, J. Cai, K. Zhang, C. Gao, L. Zhou, Z. Chen, W. Chu and D. Xia, *Energy Storage Mater.*, 2024, **71**, 103587.
68 K. Liu, Q. Zhang, Z. Lu, H. Zhu, M. Song, L. Chen, C. Zhang and W. Wei, *ACS Appl. Mater. Interfaces*, 2024, **16**, 14902–14911.
69 J. Duan, F. Wang, M. Huang, M. Yang, S. Li, G. Zhang, C. Xu, C. Tang and H. Liu, *Small*, 2024, **20**, 2307998.
70 B. E. Worku, Y. Lu, M. Song, S. Zheng and B. Wang, *Small*, 2025, **21**, 2501005.
71 Z. Ding, C. Zhang, S. Xu, J. Liu, C. Liang, L. Chen, P. Wang, D. G. Ivey, Y. Deng and W. Wei, *Energy Storage Mater.*, 2019, **21**, 69–76.

72 X. Cui, J. Zhang, C. Li, X. Cai, J. Zhou, H. Ding, J. Bai, N. Zhang, M. Wu, J. Yan, Y. Zhang and S. Li, *Acta Mater.*, 2025, **290**, 120951.
73 H. Shang, Q. He, L. Yan, E. Xiaoye and J. Xu, *Electrochim. Acta*, 2024, **503**, 144914.
74 T. Futazuka, R. Ishikawa, N. Shibata and Y. Ikuhara, *Nat. Commun.*, 2022, **13**, 5299.
75 J. Duan, F. Wang, S. Li, M. Yang, M. Huang, G. Zhang, C. Tang and H. Liu, *Chem. Eng. J.*, 2024, **489**, 151257.
76 Z. Xi, Q. Sun, J. Li, Y. Qiao, G. Min and L. Ci, *Molecules*, 2024, **29**, 1064.
77 L. Chen, Y. Su, S. Chen, N. Li, L. Bao, W. Li, Z. Wang, M. Wang and F. Wu, *Adv. Mater.*, 2014, **26**, 6756–6760.
78 C. Yang, Y. Su, W. Su, S. Ma, X. Zhu, S. Wu, Y. Li, L. Chen, D. Cao, M. Wang, Q. Huang, Y. Guan, F. Wu and N. Li, *Energy Storage Mater.*, 2025, **75**, 104019.
79 X. Zhao, C. Sheng, Z. Chang, L. Cheng, P. Wu, L. Xu, Y. Zhou, P. He, Y. Tang, X. Cao and H. Zhou, *Energy Storage Mater.*, 2025, **75**, 104093.
80 Y. Zhang, C. Yin, B. Qiu, G. Chen, Y. Shang and Z. Liu, *Energy Storage Mater.*, 2022, **53**, 763–773.
81 Z. Feng, L. Guo, X. Liu, W. Li, R. Zhang, D. Wang, W. Zhang and W. Zheng, *ACS Appl. Energy Mater.*, 2024, **7**, 2791–2799.
82 Y. Wu, C. Li, X. Zheng, W. Zhao, H. Wang, J. Gu, Y. Cheng, Y. Lin, Y. Su, F. Ren, D. Feng, J. Liu, J. Peng, Z. Lv, Z. Wang, T. Brezesinski, Z. Gong and Y. Yang, *ACS Energy Lett.*, 2024, **9**, 5156–5165.
83 J. Zhao, Y. Liang, X. Zhang, Z. Zhang, E. Wang, S. He, B. Wang, Z. Han, J. Lu, K. Amine and H. Yu, *Adv. Funct. Mater.*, 2021, **31**, 2009192.
84 W. J. Kong, C. Z. Zhao, S. Sun, L. Shen, X. Y. Huang, P. Xu, Y. Lu, W. Z. Huang, J. Q. Huang and Q. Zhang, *Adv. Mater.*, 2024, **36**, 2310738.
85 C. Shen, L. Hu, Q. Duan, X. Liu, S. Huang, Y. Jiang, W. Li, B. Zhao, X. Sun and J. Zhang, *Adv. Energy Mater.*, 2023, **13**, 2302957.
86 S. Xiao, P. Sun, Y. Xie, X. Zhou, Y. Li and L. Wang, *J. Mater. Chem. A*, 2024, **12**, 20783–20802.
87 Y. Liu, H. Liu, Y. Lin, Y. Zhao, H. Yuan, Y. Su, J. Zhang, S. Ren, H. Fan and Y. Zhang, *Adv. Funct. Mater.*, 2021, **31**, 2104863.
88 Y. Wang, D. Wu, P. Chen, P. Lu, X. Wang, L. Chen, H. Li and F. Wu, *Adv. Funct. Mater.*, 2024, **34**, 2309822.
89 Y. Chen, L. Huang, D. Zhou, X. Gao, T. Hu, Z. Zhang, Z. Zhen, X. Chen, L. Cui and G. Wang, *Adv. Energy Mater.*, 2024, **14**, 2304443.
90 O. Kwon, J. Kang, S. Kim and T. Yoon, *Adv. Funct. Mater.*, 2025, **35**, 2420474.
91 Y. Taniguchi, M. Yamamoto, A. Kato and M. Takahashi, *Solid State Ionics*, 2025, **420**, 116770.
92 S. Lee, Y. Kim, C. Park, J. Kim, J. S. Kim, H. Jo, C. J. Lee, S. Choi, D. H. Seo and S. K. Jung, *ACS Energy Lett.*, 2024, **9**, 1369–1380.
93 T. H. Hong, J. D. Kim, J. S. Lee, Y. Choi, H. Y. Jung, Y. H. Lee, S. Y. Hwang, K. Eom and J. T. Lee, *J. Mater. Chem. A*, 2024, **12**, 1998–2003.
94 M. Li, S. Yang and B. Li, *Interdiscip. Mater.*, 2024, **3**, 805–834.
95 Z. J. Cao, B. Li and S. B. Yang, *Adv. Mater.*, 2019, **31**, 1901310.
96 D. Zhang, S. Wang, B. Li, Y. J. Gong and S. B. Yang, *Adv. Mater.*, 2019, **31**, 1901820.
97 T. Wang, B. Chen, Y. Liu, Z. Song, Z. Wang, Y. Chen, Q. Yu, J. Wen, Y. Dai, Q. Kang, F. Pei, R. Xu, W. Luo and Y. Huang, *Science*, 2025, **388**, 311–316.
98 Y. Su, J. Zhao, L. Chen, N. Li, Y. Lu, J. Dong, Y. Fang, S. Chen and F. Wu, *Chin. J. Chem.*, 2021, **39**, 402–420.
99 R. Malik, V. K. Tomer and M. Sain, *EES Batteries*, 2025, **1**, 119–152.
100 Y. Han, L. Wang, K. Cao, J. Zhou, Y. Zhu, Y. Hou and Y. Lu, *Chem. Rev.*, 2023, **123**, 14119–14184.
101 J. Dong, Y. Xue, C. Zhang, Q. Weng, P. Dai, Y. Yang, M. Zhou, C. Li, Q. Cui, X. Kang, C. Tang, Y. Bando, D. Golberg and X. Wang, *Adv. Mater.*, 2017, **29**, 1603692.
102 Y. Liu, X. Su, J. Ding, J. Zhou, Z. Liu, X. Wei, H. B. Yang and B. Liu, *Chem. Soc. Rev.*, 2024, **53**, 11850–11887.
103 S. Weng, Y. Li and X. Wang, *iScience*, 2021, **24**, 103402.
104 G. Tang, J. Zhang, S. Ma, J. Li, Z. Peng and W. Chen, *Chem. Soc. Rev.*, 2025, **54**, 7216–7251.
105 Y. Fang, Y. Su, J. Dong, J. Zhao, H. Wang, N. Li, Y. Lu, Y. Wu, W. Li, N. Yang, X. Wu, F. Wu and L. Chen, *Carbon Energy*, 2025, **7**, e642.
106 J. Zhao, Y. Su, J. Dong, J. Hao, H. Che, Y. Lu, N. Li, B. Zhang, P. Zhang, F. Wu and L. Chen, *Energy Storage Mater.*, 2025, **76**, 104137.
107 Y. Li, T. Sun, C. Yang, Y. Su, C. Liu, X. Zhu, Y. Wang, S. Ma, X. Wang, Y. Zhai, W. Kang, L. Chen, M. Wang, L. Zhang, B. Wang, Q. Huang, Y. Guan, F. Wu and N. Li, *eScience*, 2025, **5**, 100405.
108 Z. Liu, Y. Zeng, J. Tan, H. Wang, Y. Zhu, X. Geng, P. Guttmann, X. Hou, Y. Yang, Y. Xu, P. Cloetens, D. Zhou, Y. Wei, J. Lu, J. Li, B. Liu, M. Winter, R. Kostecki, Y. Lin and X. He, *Nat. Nanotechnol.*, 2024, **19**, 1821–1830.
109 J. J. Marie, R. A. House, G. J. Rees, A. W. Robertson, M. Jenkins, J. Chen, S. Agrestini, M. G. Fernandez, K. J. Zhou and P. G. Bruce, *Nat. Mater.*, 2024, **23**, 818–825.
110 W. J. Kong, C. Z. Zhao, L. Shen, S. Sun, X. Y. Huang, P. Xu, Y. Lu, W. Z. Huang, J. L. Li, J. Q. Huang and Q. Zhang, *J. Am. Chem. Soc.*, 2024, **146**, 28190–28200.
111 T. Liu, J. Liu, L. Li, L. Yu, J. Diao, T. Zhou, S. Li, A. Dai, W. Zhao, S. Xu, Y. Ren, L. Wang, T. Wu, R. Qi, Y. Xiao, J. Zheng, W. Cha, R. Harder, I. Robinson, J. Wen, J. Lu, F. Pan and K. Amine, *Nature*, 2022, **606**, 305–312.
112 T. Yang, M. Yang, Z. Huang, R. Wang, W. Ji, P. H. Lu, T. Zeng, Z. Li, J. Wang, R. D. Borkowski, L. Jin and Y. Xiao, *Nat. Commun.*, 2025, **16**, 6589.
113 B. Qiu, Y. Zhou, H. Liang, M. Zhang, K. Gu, T. Zeng, Z. Zhou, W. Wen, P. Miao, L. He, Y. Xiao, S. Burke, Z. Liu and Y. S. Meng, *Nature*, 2025, **640**, 941–946.

114 Q. Zhang, J. Wang, Y. Chu, W. Huang, X. Huang, X. Xiao, L. Ma, T. Liu, K. Amine, J. Lu and C. Yang, *Nat. Energy*, 2025, **10**, 1001–1012.
115 Y. Liu, J. Dong, Y. Guan, X. Wang, Z. Chen, M. Gao, S. Guo, K. Yan, Y. Lu, M. Wang, N. Li, Y. Su, F. Wu and L. Chen, *Adv. Mater.*, 2025, e15106, DOI: 10.1002/adma.202515106.
116 M. Rittiruam, J. Noppakhun, S. Setasuban, N. Aumnongpho, A. Sriwattana, S. Boonchuay, T. Saelee, C. Wangphon, A. Ektarawong, P. Chammingkwan, T. Taniike, S. Praserthdam and P. Praserthdam, *Sci. Rep.*, 2022, **12**, 16653.
117 Y. Cao, M. Wang, M. Byeon, X. Chen, J. Choi and X. Li, *Adv. Intell. Syst.*, 2025, **7**, e202500279.
118 Y. Xie, J. Yang, Y. Cao, W. Lv, Y. B. He, L. Jiang and T. Hou, *J. Energy Chem.*, 2025, **106**, 631–641.
119 H. Huang, Y. Hu, Y. Hou, X. Wang, Q. Dong, Z. Zhao, M. Ji, W. Zhang, J. Li, J. Xie, H. Guo, X. Han, X. Ouyang and W. Hu, *Nature*, 2025, **644**, 660–667.
120 S. Wang, J. Liu, X. Song, H. Xu, Y. Gu, J. Fan, B. Sun and L. Yu, *Nano-Micro Lett.*, 2025, **17**, 287.
121 J. Kim, I. Choi, J. S. Kim, H. Hwang, B. Yu, S.-C. Nam and I. Park, *Energy Environ. Sci.*, 2025, **18**, 4222–4230.
122 J. Fan, C. Liu, N. Li, L. Yang, X. G. Yang, B. Dou, S. Hou, X. Feng, H. Jiang, H. Li, W. L. Song, L. Sun, H. S. Chen, H. Gao and D. Fang, *Nature*, 2025, **641**, 639–645.
123 Y. Sun, X. Xu, L. Gan, S. Jiao, S. Han, Y. Zhao, Y. Li, X. Yu, J. Li, H. Li and X. Huang, *EES Batteries*, 2025, **1**, 153–160.
124 Q. Meng, Y. Huang, L. Li, F. Wu and R. Chen, *Joule*, 2024, **8**, 344–373.
125 T. Zhang, J. Yu, H. Guo, J. Qi, M. Che, M. Hou, P. Jiao, Z. Zhang, Z. Yan, L. Zhou, K. Zhang and J. Chen, *Chem. Soc. Rev.*, 2024, **53**, 12043–12097.
126 A. Olgo, S. Genies, R. Franchi, C. Septet, Q. Jacquet, Q. Berrod, R. Palm, P. Chenevier, E. Villemin, C. Villevieille, N. Blanc, S. Tardif, O. Raccurt and S. Lyonnard, *Nat. Commun.*, 2024, **15**, 10258.
127 Y. Su, M. Wang, M. Zhang, L. Chen, N. Li, L. Chen, Y. Chen, J. Liu and Y. Li, *J. Alloys Compd.*, 2022, **905**, 164204.
128 J. Xiao, L. Bai, H. Qin, C. Wang, X. Gong, R. Xiong, J. Zhu, J. Zhang and X. Ou, *J. Colloid Interface Sci.*, 2025, **701**, 138668–138668.
129 K. Zhao, Y. Liu, Y. Zhou, W. Ming and J. Wu, *CSEE J. Power Energy Syst.*, 2025, **11**, 567–579.
130 K. Liu, Z. Wei, C. Zhang, Y. Shang, R. Teodorescu and Q. L. Han, *IEEE-CAA J. Autom. Sin.*, 2022, **9**, 1139–1165.
131 Y. Gao, F. Qiao, J. You, Z. Ren, N. Li, K. Zhang, C. Shen, T. Jin and K. Xie, *Nat. Commun.*, 2022, **13**, 5.
132 M. Tian, Y. Yan, H. Yu, L. Ben, Z. Song, Z. Jin, G. Cen, J. Zhu, M. Armand, H. Zhang, Z. Zhou and X. Huang, *Adv. Mater.*, 2024, **36**, 2400707.
133 C. X. Zhao, Z. Li, B. Chen, F. Chen and C. Wang, *Nat. Energy*, 2025, **10**, 904–913.
134 C. Lv, X. Zhou, L. Zhong, C. Yan, M. Srinivasan, Z. W. Seh, C. Liu, H. Pan, S. Li, Y. Wen and Q. Yan, *Adv. Mater.*, 2022, **34**, 2101474.
135 Y. Liu, A. Madanchi, A. S. Anker, L. Simine and V. L. Deringer, *Nat. Rev. Mater.*, 2025, **10**, 228–241.